AAPPS Bulletin

ORIGINAL ARTICLE

Open Access

Magnetic-resonance-induced non-linear current response in magnetic Weyl semimetals

Ruobing Mei[1] and Chao-Xing Liu[1*]

Abstract

In this work, we propose a geometric non-linear current response induced by magnetic resonance in magnetic Weyl semimetals. This phenomenon is in analog to the quantized circular photogalvanic effect (de Juan et al., Nat. Commun. 8:15995, 2017) previously proposed for Weyl semimetal phases of chiral crystals. However, the non-linear current response in our case can occur in magnetic Weyl semimetals where time-reversal symmetry, instead of inversion symmetry, is broken. The occurrence of this phenomenon relies on the special coupling between Weyl electrons and magnetic fluctuations induced by magnetic resonance. To further support our analytical solution, we perform numerical studies on a model Hamiltonian describing the Weyl semimetal phase in a topological insulator system with ferromagnetism.

1 Introduction

Topological and geometric aspects of electronic Bloch wavefunctions in the Brillouin zone (BZ), including the Berry curvature [1–3] and quantum metric [3–6], play essential roles in our understanding of physical responses in crystalline materials. For example, the Hall conductivity of a 2D crystalline insulator can be related to the integral of the momentum-space Berry curvature for the Bloch wavefunctions over the entire BZ, which is identified as a topological index called the "Chern number" in the formula first derived by Thouless, Kohmoto, Nightingale, and den Nijs [7]. The Berry curvature integral of the occupied states, which is not quantized, also provides an intrinsic mechanism for the anomalous Hall effect in a variety of ferromagnetic metals. More recently, physical phenomena induced by non-linear responses have also been connected to band topology or geometry. For example, the Berry curvature dipole and quantum metric dipole are theoretically proposed to be the origin of the non-linear Hall effect in non-magnetic or anti-ferromagnetic materials, which preserve either time-reversal symmetry ($\hat{T}$) or the combined $\hat{P}\hat{T}$-symmetry where $\hat{P}$ is inversion [8–13]. This geometric origin of non-linear Hall effect has been experimentally demonstrated in a variety of material compounds [14–25]. Quantized topological non-linear response due to chiral charges of Weyl nodes has also been theoretically proposed for the circular photogalvanic effect (CPGE) in Weyl semimetals [26–28]. Experimental observation of CPGE has been reported in chiral multifold semimetals RhSi and CoSi and its connection to topological chiral charges has been discussed [29–31].

The CPGE is a second-order optical response, in which the current switches its direction when the circularly polarized incident light changes its polarization [27–34]. In Ref. [27], de Juan et al. proposed that the CPGE can be quantized in the Weyl semimetal phase of chiral crystals and this quantization originates from the topological chiral charge of Weyl nodes. Because the Weyl nodes must appear in pairs with opposite chiral charges in crystals, the CPGE contributions from the Weyl nodes with opposite chiral charges will cancel each other, generally leading to the vanishing CPGE (Fig. 1a). To overcome this obstruction, it was theoretically proposed that when two Weyl nodes with opposite chiral charges sit at different energies and the Fermi energy is close to

*Correspondence:
Chao-Xing Liu
cxl56@psu.edu
[1] Department of Physics, The Pennsylvania State University, University Park, PA 16802, USA

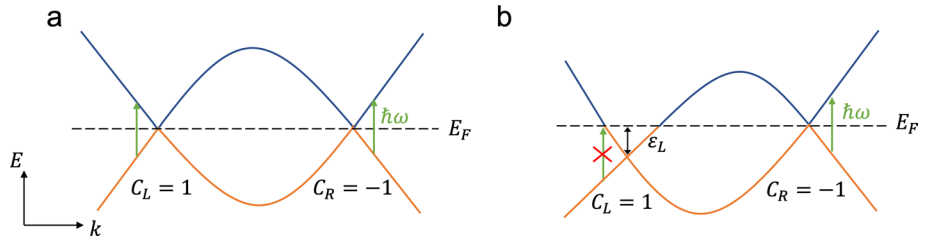

Fig. 1 **a** Schematic of the energy dispersion for a two-band Weyl semimetal that preserves mirror symmetry and breaks time-reversal symmetry. The left and right Weyl nodes have opposite *C* and sit at the same energy. The current response of topological CPGE will cancel out between these two Weyl nodes due to the opposite chiral charges, but the magnetic-resonance-induced non-linear current proposed in this work will remain. **b** Band structure of a chiral Weyl semimetal where the two Weyl nodes are at different energies. The topological CPGE can exist due to Pauli blocking

one Weyl node but far away from the other Weyl node (Fig. 1b), optical inter-band transitions can only occur for the Weyl fermion close to the Fermi energy but not for the other due to Pauli blocking [27]. This scenario can occur in the Weyl semimetal phase of chiral crystals, in which the inversion and all the mirror symmetries are broken, so that no symmetry can connect the Weyl nodes with opposite chiral charges, and thus they can appear at different energies. We note that time-reversal symmetry can only relate two Weyl nodes with the same chiral charge. However, experimental confirmation of quantized CPGE is still lacking, and it was suggested that additional contributions from remote bands, rather than the two bands that form Weyl fermions, can have a significant contribution to the CPGE, which can be much larger than the quantized contribution in realistic materials [35]. Furthermore, it was also suggested that interactions and disorders can destroy the quantization of CPGE in chiral Weyl semimetals [36, 37].

In this work, we propose an alternative approach to overcome this obstruction in magnetic Weyl semimetals, in which time-reversal symmetry is broken but inversion symmetry is preserved. The current response from the second order (or any even order) of electric fields (E^2) necessarily requires inversion symmetry breaking, which directly follows from the fact that both current and electric field are odd under inversion. Following this argument, the CPGE contributions from different Weyl nodes in centrosymmetric magnetic Weyl semimetals will cancel each other so that we expect a vanishing CPGE for the second-order response (Fig. 1a). The key idea in our approach is to replace one electric field E with magnetization M, which is even under inversion. Therefore, the second-order current response with respect to one magnetization M and one electric field E is allowed to exist in centrosymmetric magnetic Weyl semimetals from the symmetry view. Microscopically, to understand how magnetization dynamics affects the inter-band transition of Weyl fermions, we introduce the concept of "pseudo-gauge field" in magnetic Weyl semimetals and show that magnetic fluctuations (or spin wave) can play the role of a pseudo-gauge field[38–40]. Here the pseudo-gauge field refers to the perturbation that behaves in a similar manner as a gauge field coupled to the Weyl fermions in the low-energy sector of the system. Unlike the usual electromagnetic field, this gauge coupling depends on the chirality of Weyl fermions and has opposite signs when the Weyl fermion chirality reverses. In Section 3, we will study the non-linear current response in magnetic Weyl semimetals due to the interplay between electromagnetic fields and the magnetic-resonance (MR) induced pseudo-gauge field, in analogy to the CPGE purely from the electromagnetic fields. Strikingly, we find that two Weyl nodes with opposite chiral charges contribute with the same sign to the MR-induced nonlinear current, in sharp contrast to the opposite sign contributions of the normal CPGE. This difference originates from the chirality-dependent gauge coupling form of the pseudo-gauge field. In Section 4, we will demonstrate that the magnetic fluctuation or spin wave, which can be driven via ferromagnetic resonance, serves as the pseudo-gauge field in magnetic Weyl semimetals. In Section 5, we implemented numerical studies of the magnetic-resonance-induced nonlinear current response in a magnetic Weyl semimetal model that was previously adopted to describe magnetically doped topological insulators, in order to justify our analytical solutions.

2 Model Hamiltonian

We start from a four-band model that describe a topological insulator system with ferromagnetism in Ref. [41], which can capture the Weyl semimetal phase when magnetization term dominates over the non-magnetic band gap. The model Hamiltonian reads

$$\begin{aligned} H &= H_0 + H_1, \\ H_0 &= \mathcal{M}(\boldsymbol{k})\tau_z + L_1 k_z \tau_y + L_2(k_y\sigma_x - k_x\sigma_y)\tau_x + m\sigma_z, \\ H_1 &= \boldsymbol{v}(t)\cdot\boldsymbol{\sigma}\tau_z, \end{aligned} \tag{1}$$

where $\mathcal{M}(\boldsymbol{k}) = M_0 + M_1 k_z^2 + M_2(k_x^2 + k_y^2)$, $M_{0,1,2}, L_{1,2}$ are material dependent parameters, and m describes the out-of-plane magnetization and can induce the Weyl semimetal phase when $m > M_0$ after neglecting the quadratic terms in $\mathcal{M}(\boldsymbol{k})$. Here we also include the H_1 term that represents the magnetic fluctuation, which preserves the inversion symmetry τ_z and breaks the time-reversal $i\sigma_y K$ (K is the complex conjugate operator), and assume $\boldsymbol{\nu}(t)$ has temporal dependence. In Ref. [41], additional terms with the form $\boldsymbol{\mu}(t)\cdot\boldsymbol{\sigma}$ can exist for magnetic fluctuations. However, these terms will only slightly modify the form of the pseudo-gauge field discussed below and does not affect the final result. Thus, we drop these additional terms and only focus on the $\boldsymbol{\nu}(t)$ terms in this work. H_1 is treated as a perturbation below. Next we will show that when the model Hamiltonian is in the magnetic Weyl semimetal phase for $m > M_0$ and projected to the subspace of two low-energy Weyl fermions, the magnetic fluctuation in H_1 acts like a chiral gauge field which couples oppositely to the Weyl fermions with left and right chiralities [41].

The eigen-energy of the Hamiltonian H_0 in Eq. (1) can be solved analytically as

$$\varepsilon_{\lambda\mu} = \lambda\sqrt{L_2^2\left(k_x^2+k_y^2\right) + \left(\sqrt{\mathcal{M}^2 + L_1^2 k_z^2} + \mu|m|\right)^2}, \tag{2}$$

where $\lambda, \mu = \pm$, and we denote the eigenstates as $|\lambda, \mu\rangle$. When $k_x = k_y = 0$, the eigen-energies of the two middle bands are $\varepsilon_{-,-} = -\sqrt{\mathcal{M}^2 + L_1^2 k_z^2} + m$ and $\varepsilon_{+,-} = \sqrt{\mathcal{M}^2 + L_1^2 k_z^2} - m$, assuming $m > 0$. Thus, the gap between the two states $|-,-\rangle$ and $|+,-\rangle$ can be closed at $\mathcal{M}^2 + L_1^2 k_z^2 = m^2$ if $m > |\mathcal{M}|$. By neglecting the quadratic term $M_1 k_z^2$ in $\mathcal{M}(\boldsymbol{k})$, namely $\mathcal{M}(\boldsymbol{k}) = M_0$, we can find two gap closing points at $\boldsymbol{k} = (0, 0, \pm K_0)$ with $K_0 = \sqrt{m^2 - M_0^2}/L_1$.

At the gap closing point $\boldsymbol{k}_0 = (0, 0, K_0)$, the Hamiltonian can be simplified as

$$H_0(\boldsymbol{k}_0) = M_0\tau_z + L_1 K_0 \tau_y + m\sigma_z, \tag{3}$$

and the eigenstates are solved as

$$\begin{aligned}
|-,+\rangle &= \frac{1}{\sqrt{N_-}}\begin{pmatrix} 0 \\ 0 \\ M_0 - m \\ iL_1K_0 \end{pmatrix}, \quad |-,-\rangle = \frac{1}{\sqrt{N_-}}\begin{pmatrix} M_0 - m \\ iL_1K_0 \\ 0 \\ 0 \end{pmatrix}, \\
|+,-\rangle &= \frac{1}{\sqrt{N_+}}\begin{pmatrix} 0 \\ 0 \\ M_0 + m \\ iL_1K_0 \end{pmatrix}, \quad |+,+\rangle = \frac{1}{\sqrt{N_+}}\begin{pmatrix} M_0 + m \\ iL_1K_0 \\ 0 \\ 0 \end{pmatrix},
\end{aligned} \tag{4}$$

where $N_\pm = (M_0 \pm m)^2 + L_1^2 K_0^2$ are the normalization factors. The effective Hamiltonian around $\boldsymbol{k}_0$ up to the first order in $\delta\boldsymbol{k}$ is written as

$$H' = L_1\delta k_z\tau_y + L_2(\delta k_y\sigma_x - \delta k_x\sigma_y)\tau_x + \boldsymbol{\nu}\cdot\boldsymbol{\sigma}\tau_z. \tag{5}$$

We then project the effective Hamiltonian H' into the subspace of the basis $|-,-\rangle$ and $|+,-\rangle$ by applying the second-order perturbation

$$H_{mn} = \langle m|H'|n\rangle + \sum_{l\neq m,n}\frac{1}{2}\langle m|H'|l\rangle\langle l|H'|n\rangle\times\left[\frac{1}{\varepsilon_m - \varepsilon_l} + \frac{1}{\varepsilon_n - \varepsilon_l}\right]. \tag{6}$$

By keeping $\delta\boldsymbol{k}$ up to the first order and $\boldsymbol{\nu}$ up to the second order, we can then write down the low-energy effective Hamiltonian for the two gap closing points at $(0, 0, K_0)$ and $(0, 0, -K_0)$ as

$$\begin{aligned}
H_{\mathit{eff}} &= \left(L_2\delta k_x\tau_z + \frac{L_1K_0}{m}\nu_x\right)\sigma_x + \left(L_2\delta k_y\tau_z + \frac{L_1K_0}{m}\nu_y\right)\sigma_y \\
&\quad + \frac{1}{2m}\left(2L_1^2K_0\delta k_z\tau_z - \nu_z^2 + \frac{M_0^2}{m^2}(\nu_x^2+\nu_y^2+\nu_z^2)\right)\sigma_z \\
&= \hbar v_f\boldsymbol{\sigma}\cdot\left(\delta\boldsymbol{k}\,\tau_z + \frac{e}{\hbar}\boldsymbol{a}\right),
\end{aligned} \tag{7}$$

where $\boldsymbol{\sigma}$ are Pauli matrices in the spin basis, τ_z is in the basis of two Weyl points, $\hbar v_f = L_2$, $\delta\boldsymbol{k} = (\delta k_x, \delta k_y, \frac{L_1^2K_0}{L_2 m}\delta k_z)$, and $\boldsymbol{a} = (a_x, a_y, a_z)$ with $a_x = \frac{\hbar L_1 K_0}{eL_2 m}\nu_x$, $a_y = \frac{\hbar L_1 K_0}{eL_2 m}\nu_y$, and $a_z = \frac{\hbar}{2eL_2 m}(-\nu_z^2 + \frac{M_0^2}{m^2}(\nu_x^2+\nu_y^2+\nu_z^2))$. We may introduce the electromagnetic field by the Peierls substitution $\delta\boldsymbol{k} \to \delta\boldsymbol{k} + \frac{e}{\hbar}\boldsymbol{A}$ with the vector potential $\boldsymbol{A}$. By comparing the coupling form of $\boldsymbol{A}$ with $\boldsymbol{a}$, we find that the $\boldsymbol{a}$ field, which results from the magnetic fluctuation $\boldsymbol{\nu}$, couples oppositely to the Weyl nodes at the two gap closing points in a gauge coupling form, and thus we conclude the $\boldsymbol{a}$ field acts like a chiral gauge field [41]. Below we will use the terminology, either chiral gauge field or pseudo-gauge field, to refer to the $\boldsymbol{a}$ field.

Due to the presence of magnetic ordering, time-reversal symmetry is broken in magnetic Weyl semimetals, and the minimal model of Weyl semimetals with two Weyl nodes can be realized by the model Hamiltonian in Eq. (1), as shown by the numerical simulations of the energy bands for Eq. (1) in Fig. 2a. On the other hand, if only inversion symmetry is broken, the total number of Weyl nodes in the system must be a multiple of four, as time-reversal symmetry transforms a Weyl node at $\boldsymbol{k}$ to another Weyl node at $-\boldsymbol{k}$ with the same chirality and all the chiral charges for the whole Weyl semimetals must cancel [42].

3 Magnetic-resonance-induced current response for Weyl fermions

We next consider the non-linear response for the left-handed and right-handed Weyl fermions described by the Hamiltonian based on the effective Hamiltonian Eq. (7) which is rewritten as

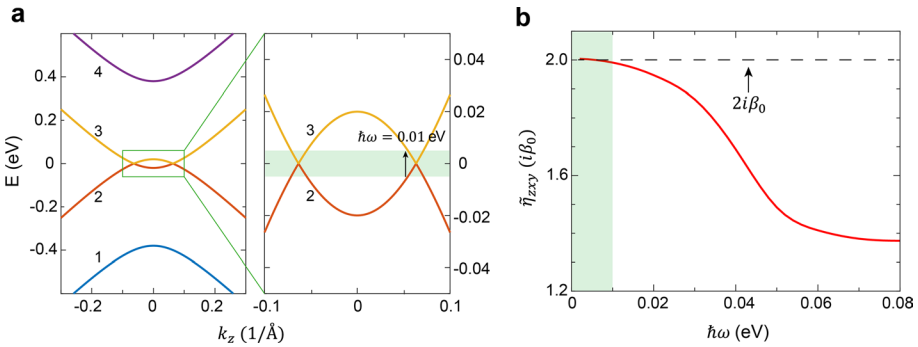

Fig. 2 **a** Energy dispersion of the four-band model along k_z at $k_x = k_y = 0$ and the enlarged area around the two Weyl nodes. **b** The MR-induced non-linear current component $\tilde{\eta}_{zxy}$ as a function of $\hbar\omega$. The quantized value is $2i\beta_0$, which can be achieved for $\hbar\omega < 0.01$ eV. The parameters are chosen as $M_0 = 0.18$ eV, $M_1 = 0.342$ eVÅ^2, $M_2 = 18.25$ eVÅ^2, $L_1 = 1.33$ eVÅ, $L_2 = 2.82$ eVÅ, and $m = 0.2$ eV (parameters from Ref. [41])

$$\begin{aligned} H_L &= \hbar v_f \boldsymbol{\sigma}\cdot\left(\boldsymbol{k}+\frac{e}{\hbar}\boldsymbol{A}+\frac{e}{\hbar}\boldsymbol{a}\right),\\ H_R &= -\hbar v_f \boldsymbol{\sigma}\cdot\left(\boldsymbol{k}+\frac{e}{\hbar}\boldsymbol{A}-\frac{e}{\hbar}\boldsymbol{a}\right), \end{aligned} \tag{8}$$

where $\boldsymbol{\sigma}$ is Pauli matrices, $\boldsymbol{A}$ is the electromagnetic field, and $\boldsymbol{a}$ is the chiral gauge field minimally coupled to the left-handed and right-handed Weyl fermions [41]. We further rewrite the above Hamiltonian as

$$\begin{aligned} H_L &= H_{L0} + \boldsymbol{A}\cdot\boldsymbol{J}_L + \boldsymbol{a}\cdot\boldsymbol{J}_L,\\ H_R &= H_{R0} + \boldsymbol{A}\cdot\boldsymbol{J}_R - \boldsymbol{a}\cdot\boldsymbol{J}_R, \end{aligned} \tag{9}$$

where $H_{L0} = -H_{R0} = \hbar v_f \boldsymbol{\sigma}\cdot\boldsymbol{k}$ and $\boldsymbol{J}_L = -\boldsymbol{J}_R = e v_f \boldsymbol{\sigma}$. Let us first focus on the left-handed Weyl fermion H_L. Following the density matrix formalism in the velocity gauge described in Appendix 2, we rewrite the Hamiltonian into the second-quantization form as

$$\hat{H}_L = \sum_n \int d\boldsymbol{k}\varepsilon^L_{n\boldsymbol{k}}\hat{a}^\dagger_{n\boldsymbol{k}}\hat{a}_{n\boldsymbol{k}} + \sum_{nn'}\int d\boldsymbol{k}\hat{a}^\dagger_{n\boldsymbol{k}}\hat{a}_{n'\boldsymbol{k}}\left[\boldsymbol{A}(t)\cdot\boldsymbol{J}^L_{nn'\boldsymbol{k}} + \boldsymbol{a}_L(t)\cdot\boldsymbol{J}^L_{nn'\boldsymbol{k}}\right], \tag{10}$$

where $\varepsilon^L_{n\boldsymbol{k}}$ is the eigenvalue of H_{L0} and $\hat{a}_{n\boldsymbol{k}}$ and $\hat{a}^\dagger_{n\boldsymbol{k}}$ are the annihilation and creation operators. The Bloch equation of the density matrix $\rho_{nm}(t)$, defined by $\rho_{nm,\boldsymbol{k}}(t) = \langle\hat{a}^\dagger_{m\boldsymbol{k}}(t)\hat{a}_{n\boldsymbol{k}}(t)\rangle$, is then

$$\begin{aligned} \frac{\partial\rho_{nm}(t)}{\partial t} &= -\frac{i}{\hbar}\varepsilon^L_{nm}\rho_{nm}(t) - \frac{i}{\hbar}\sum_{n'}\left[\boldsymbol{A}(t)\cdot\boldsymbol{J}^L_{n'n}\rho_{n'm}(t) - \boldsymbol{A}(t)\cdot\boldsymbol{J}^L_{mn'}\rho_{nn'}(t)\right]\\ &\quad -\frac{i}{\hbar}\sum_{n'}\left[\boldsymbol{a}_L(t)\cdot\boldsymbol{J}^L_{n'n}\rho_{n'm}(t) - \boldsymbol{a}_L(t)\cdot\boldsymbol{J}^L_{mn'}\rho_{nn'}(t)\right] - \frac{\rho_{nm}(t)}{\tau}, \end{aligned} \tag{11}$$

where τ is the relaxation time and $\varepsilon^L_{nm} = \varepsilon^L_n - \varepsilon^L_m$. We can expand the density matrix in order of the perturbation of dynamic fields $\boldsymbol{A}$ and $\boldsymbol{a}$. The zeroth order of the density matrix is given by $\rho^{(0)}_{nm} = f_n\delta_{nm}$ where f_n is the Fermi factor of band n. At the first order of $\boldsymbol{A}$ and $\boldsymbol{a}$, we obtain

$$\rho^{(1)}_{nm}(\omega) = f_{nm}\frac{\left(A^b(\omega) + a^b_L(\omega)\right)(J_L)^b_{mn}}{\hbar(\tilde{\omega}_{1,nm} - \omega)}, \tag{12}$$

where we define $f_{nm} = f_n - f_m$, $A^b(t) = A^b(\omega)e^{-i\omega t}$, $a^b_L(t) = a^b_L(\omega)e^{-i\omega t}$, and $\tilde{\omega}_{1,nm} = \varepsilon^L_{nm}/\hbar - i/\tau$. Here the Einstein summation rule has been assumed. At the second order of $\boldsymbol{A}$ and $\boldsymbol{a}$, the diagonal component of density matrix can be derived as

$$\rho^{(2)}_{nn}(\omega_\Sigma) = \frac{1}{\hbar\omega_\Sigma}\sum_m\left(A^b_\beta(a_L)^c_\gamma + (a_L)^b_\beta A^c_\gamma\right)\left[\frac{f_{mn}(J_L)^b_{mn}(J_L)^c_{mn}}{\hbar(\tilde{\omega}_{1,mn} - \omega_\beta)} - \frac{f_{nm}(J_L)^b_{nm}(J_L)^c_{mn}}{\hbar(\tilde{\omega}_{1,mn} - \omega_\beta)}\right], \tag{13}$$

where $\omega_\Sigma = \omega_\beta + \omega_\gamma$, $A^b_\beta = A^b(\omega_\beta)$, and $(a_L)^b_\beta = (a_L)^b(\omega_\beta)$. Here we only consider the diagonal term in the second order of density matrix $\rho^{(2)}$. This is because we only consider two bands that form the Weyl points here, and the off-diagonal component of $\rho^{(2)}$ is zero. It should be noted that if the third bands are involved, the off-diagonal component of $\rho^{(2)}$ can exist and a three-band contribution can be important for the CPGE [35]. Moreover, we only keep the terms involving both $\boldsymbol{A}$ and $\boldsymbol{a}_L$, as the other terms quadratic in $\boldsymbol{A}$ or $\boldsymbol{a}_L$ vanish between the left-handed and right-handed Weyl fermions due to their opposite chiral charges (see Appendix 1). The corresponding intraband current is derived as

$$\begin{aligned} \tilde{j}^a_L(t) &= e\sum_n\int_k v^a_{nn}\rho^{(2)}_{nn}(\omega_\Sigma)e^{-i\omega_\Sigma t}\\ &= \frac{e}{\hbar^2\omega_\Sigma}\sum_{nm}\int_k\frac{\Delta^a_{nm}f_{mn}(J_L)^b_{mn}(J_L)^c_{nm}}{\tilde{\omega}_{1,mn} - \omega_\beta}\left(A^b_\beta(a_L)^c_\gamma + (a_L)^b_\beta A^c_\gamma\right)e^{-i\omega_\Sigma t}, \end{aligned} \tag{14}$$

where $v^a_{nm} = \langle n|\frac{\partial H}{\partial k_a}|m\rangle$ is the matrix element of the velocity operator and $\Delta^a_{nm} = v^a_{nn} - v^a_{mm}$ is the velocity shift. We then use $A^b(\omega) = E^b(\omega)/i\omega$, $a^b_L(\omega) = \tilde{E}^b(\omega)/i\omega$ with the pseudo-electric field $\tilde{E}$, and $(J_L)^b_{nm} = \frac{ie}{\hbar}\varepsilon^L_{nm}\mathcal{A}^b_{nm}$ with the Berry connection $\boldsymbol{\mathcal{A}}_{nm} = \langle n|i\partial_{\boldsymbol{k}}|m\rangle$. We symmetrize all the indices, and take the time derivative of the imaginary part (see Appendix 1) to obtain

$$\frac{d\tilde{j}_L^a(t)}{dt} = \tilde{\eta}^L_{abc}(\omega_\Sigma;\omega_\beta,\omega_\gamma)E^b_\beta \tilde{E}^c_\gamma e^{-i\omega_\Sigma t} + \tilde{\eta}^L_{abc}(\omega_\Sigma;\omega_\gamma,\omega_\beta)\tilde{E}^b_\beta E^c_\gamma e^{-i\omega_\Sigma t}, \quad (15)$$

where

$$\tilde{\eta}^L_{abc}(\omega_\Sigma;\omega_\beta,\omega_\gamma) = -\frac{i\pi e^3}{8\hbar^2}\sum_{nm}\int_k \Delta^a_{nm} f_{nm}(\Omega_L)^{bc}_{mn}\frac{\varepsilon^2_{nm}}{\hbar^2\omega_\beta\omega_\gamma} \times \left[\delta(\omega_{mn}-\omega_\beta)-\delta(\omega_{mn}+\omega_\beta)-\delta(\omega_{mn}-\omega_\gamma)+\delta(\omega_{mn}+\omega_\gamma)\right], \quad (16)$$

with the Berry curvature of the left-handed Weyl fermion $(\Omega_L)^{bc}_{mn} = i(\mathcal{A}^b_{mn}\mathcal{A}^c_{nm} - \mathcal{A}^c_{mn}\mathcal{A}^b_{nm})$. For $\omega_\beta = -\omega_\gamma = \omega$ and $\omega_\Sigma = 0$, we have

$$\tilde{\eta}^L_{abc}(0;\omega,-\omega) = -\frac{i\pi e^3}{2\hbar^2}\sum_{nm}\int_k \Delta^a_{nm} f_{nm}(\Omega_L)^{bc}_{mn}\delta(\omega_{mn}-\omega). \quad (17)$$

We rewrite the above equations as (see Appendix 1)

$$\tilde{\boldsymbol{j}}_L = \tau\tilde{\beta}_L(\omega)\left[\boldsymbol{E}(\omega)\times\tilde{\boldsymbol{E}}^*(\omega) + \tilde{\boldsymbol{E}}(\omega)\times\boldsymbol{E}^*(\omega)\right], \quad (18)$$

where $\tilde{\boldsymbol{E}}(\omega) = i\omega\boldsymbol{a}$ can be regarded as the pseudo-electric field, and the MR-induced current response trace for the left-handed Weyl fermion is

$$\tilde{\beta}_L(\omega) = i\frac{e^3}{2h^2}\oint d\boldsymbol{S}\cdot\boldsymbol{\Omega}_L = i\beta_0 C_L, \quad (19)$$

where $\boldsymbol{S}$ is a closed surface in the momentum space, $\beta_0 = \pi e^3/h^2$, and $C_L = \frac{1}{2\pi}\oint d\boldsymbol{S}\cdot\boldsymbol{\Omega}_L = 1$ is nothing but the Chern number (equivalently the chiral charge of the Weyl node). For the right-handed Weyl fermion with $C_R = -C_L$, we repeat the above derivation to obtain $\tilde{\boldsymbol{j}}_R = \tilde{\boldsymbol{j}}_L$. Thus, the total non-linear response current is

$$\tilde{\boldsymbol{j}} = \tilde{\boldsymbol{j}}_L + \tilde{\boldsymbol{j}}_R = 2i\tau\beta_0 C_L\left[\boldsymbol{E}(\omega)\times\tilde{\boldsymbol{E}}^*(\omega) + \tilde{\boldsymbol{E}}(\omega)\times\boldsymbol{E}^*(\omega)\right]. \quad (20)$$

The current Eq. (20) is the main result of this work, from which we demonstrate that a non-zero total *dc*-current can be induced by the interplay between an electromagnetic field and a chiral gauge field at the non-linear order for two Weyl nodes with opposite chiral charges, in contrast to the regular CPGE as discussed in Appendix 1 (also see Ref. [27]). Furthermore, the symmetry properties of each component in Eq. (20) are summarized in Table 1. Unlike the physical electric field E, the pseudo-electric field $\tilde{E}$ is even under inversion. Therefore, this current response is allowed in centrosymmetric systems, i.e., when the inversion symmetry is preserved. From Eq. (7), we can see that the chiral gauge field $\boldsymbol{a}$ depends on the time-dependent field $\boldsymbol{v}(t)$ that describes magnetic fluctuations and thus we study the magnetic dynamics in magnetic topological insulators below.

4 Landau-Lifshitz-Gilbert equation for ferromagnetic resonance

To see how the magnetic fluctuation can induce a pseudo-electric field, we solve the Landau-Lifshitz-Gilbert (LLG) equation for ferromagnetic resonance in this section. Similar to Ref. [38], the LLG equation reads

$$\frac{d\boldsymbol{M}}{dt} = -\gamma_0\boldsymbol{M}\times\left(\boldsymbol{B}_{\text{eff}} - \eta\frac{d\boldsymbol{M}}{dt}\right), \quad (21)$$

where $\boldsymbol{M} = (M_x, M_y, M_z)$ is the magnetization. The in-plane magnetization acts as a pseudo-gauge field in terms of $\boldsymbol{v} = \frac{c}{ev_f}g_M(-M_y, M_x, 0)$, with the exchange coupling coefficient g_M [38]. Therefore, the pseudo-electric field induced by the ferromagnetic resonance is

$$\tilde{\boldsymbol{E}} = -\frac{1}{c}\frac{\partial\boldsymbol{v}}{\partial t} = \frac{g_M}{ev_f}\left(\frac{dM_y}{dt}, -\frac{dM_x}{dt}, 0\right). \quad (22)$$

The LLG equation can be rewritten as

$$\begin{aligned}\frac{d\boldsymbol{M}}{dt} &= -\gamma_0\boldsymbol{M}\times\left[\boldsymbol{B}_{\text{eff}} - \eta\left(-\gamma_0\boldsymbol{M}\times\left(\boldsymbol{B}_{\text{eff}} - \eta\frac{d\boldsymbol{M}}{dt}\right)\right)\right] \\ &\approx -\gamma_0\boldsymbol{M}\times\boldsymbol{B}_{\text{eff}} - \eta\gamma_0^2\boldsymbol{M}\times(\boldsymbol{M}\times\boldsymbol{B}_{\text{eff}}),\end{aligned} \quad (23)$$

where $\boldsymbol{B}_{\text{eff}} = \boldsymbol{B} - \boldsymbol{M}_N - \frac{KM_z}{M_s^2}\hat{e}_z$, $\boldsymbol{B}$ is the applied magnetic field, $M_s = |\boldsymbol{M}|$, K is the anisotropy coefficient, $\boldsymbol{M}_N = (N_xM_x, N_yM_y, N_zM_z)$ is the demagnetizing field with $N_x, N_y = 0$ and $N_z = 1$ as we consider a thin film perpendicular to the z direction, $\gamma_0 = \frac{ge}{2m_e}$ is the magneto-mechanical ratio with Landé factor g, and η is Gilbert damping coefficient [38, 43, 44]. Let us define the dimensionless damping constant $\alpha = \gamma_0\eta M_s$, $\gamma = \frac{\gamma_0}{1+\alpha^2}$, and the LLG equation is written as

$$\frac{d\boldsymbol{M}}{dt} = -\gamma\boldsymbol{M}\times\boldsymbol{B}_{\text{eff}} - \frac{\gamma\alpha}{M_s}\boldsymbol{M}\times(\boldsymbol{M}\times\boldsymbol{B}_{\text{eff}}). \quad (24)$$

Table 1 Symmetry properties of current $\tilde{j}$, relaxation time τ, electric field E, and pseudo-electric field $\tilde{E}$ (+ for even and − for odd)

	$\tilde{j}$	τ	$\boldsymbol{E}$	$\tilde{E}$
Inversion	−	+	−	+
Time-reversal	−	−	+	+

Since $dM_s/dt = 0$, only the direction $\boldsymbol{n} = \boldsymbol{M}/M_s$ is time-dependent with

$$\frac{d\boldsymbol{n}}{dt} = -\gamma \boldsymbol{n} \times \boldsymbol{B}_{\text{eff}} - \gamma\alpha \boldsymbol{n} \times (\boldsymbol{n} \times \boldsymbol{B}_{\text{eff}}). \tag{25}$$

We assume the in-plane magnetic field and magnetization are very small, i.e. $|n_x| \sim |n_y| \sim |B_x/M_s| \sim |B_y/M_s| \ll 1$, and at the first order of these quantities, we have

$$\begin{pmatrix} \partial_t + \alpha\tilde{\omega} & \tilde{\omega} n_z \\ -\tilde{\omega} n_z & \partial_t + \alpha\tilde{\omega} \end{pmatrix} \begin{pmatrix} n_x \\ n_y \end{pmatrix} = \begin{pmatrix} \gamma\alpha & \gamma n_z \\ -\gamma n_z & \gamma\alpha \end{pmatrix} \begin{pmatrix} B_x \\ B_y \end{pmatrix}, \tag{26}$$

where $\tilde{\omega} = \gamma n_z B_{\text{eff},z}$ and $n_z = M_z/M_s = \text{sgn}(M_z)$. We then consider a general in-plane magnetic field $\boldsymbol{B}(t) = B_0 e^{i\omega t}(a, b, 0)$ where a, b are two complex numbers and describe the polarization of magnetic field components of a microwave. By performing the Laplace transformation in Appendix 4, we keep the leading order $\mathcal{O}(\alpha^{-1})$ in Eqs. (101) and (102) to get

$$\begin{aligned} n_x(t) &= \frac{B_0\gamma_0}{2\alpha\omega_0}[(a_{\text{Im}} + b_{\text{Re}} n_z)\cos(\omega_0 t) + (a_{\text{Re}} - b_{\text{Im}} n_z)\sin(\omega_0 t)], \\ n_y(t) &= \frac{B_0\gamma_0}{2\alpha\omega_0}[(b_{\text{Im}} - a_{\text{Re}} n_z)\cos(\omega_0 t) + (b_{\text{Re}} + a_{\text{Im}} n_z)\sin(\omega_0 t)], \end{aligned} \tag{27}$$

where the ferromagnetic resonance frequency is

$$\omega_0 = |\tilde{\omega}| = \gamma B_{\text{eff},z} \tag{28}$$

by taking the leading order $\mathcal{O}(\alpha^{-1})$ in ω_r (Eq. (104)), and Re and Im denote the real and imaginary parts of a and b, respectively. Therefore, from Eq. (22), the pseudo-electric field reads

$$\begin{aligned} \tilde{E}_x &= \frac{g_M}{e v_f}\frac{dM_y}{dt} = \frac{g_M M_s}{e v_f}\dot{n}_y = \tilde{E}_0(b - i a n_z)e^{i\omega_0 t}, \\ \tilde{E}_y &= -\frac{g_M}{e v_f}\frac{dM_x}{dt} = -\frac{g_M M_s}{e v_f}\dot{n}_x = -\tilde{E}_0(a + i b n_z)e^{i\omega_0 t}, \end{aligned} \tag{29}$$

where $\tilde{E}_0 = g_M B_0/(2 e v_f \eta)$. Thus, an in-plane magnetic field $\boldsymbol{B}(t) = B_0 e^{i\omega_0 t}(a, b, 0)$ can induce a pseudo-electric field

$$\tilde{\boldsymbol{E}}(t) = \tilde{E}_0 e^{i\omega_0 t}(b - i a n_z, -a - i b n_z, 0), \tag{30}$$

where $n_z = \text{sgn}(M_z)$. Combining Eq. (30) with Eq. (20) for the non-linear current response and considering an incident light with $\boldsymbol{E}(t) = E_0 e^{i\omega_0 t}(c, d, 0)$, we find

$$\begin{aligned} \tilde{\boldsymbol{j}} &= 2i\tau\beta_0 C_L E_0 \tilde{E}_0 \big[(-a^* + i b^* n_z)c - (b^* + i a^* n_z)d - (-a - i b n_z)c^* + (b - i a n_z)d^*\big]\hat{e}_z \\ &= -4\tau\beta_0 C_L E_0 \tilde{E}_0 \text{Im}\big[(-a^* + i b^* n_z)c - (b^* + i a^* n_z)d\big]\hat{e}_z. \end{aligned} \tag{31}$$

Because the MR-induced non-linear current response is generated by the combination of an electromagnetic field and a pseudo-electric field, the incident light can be linearly polarized, instead of circularly polarized which is required for the regular CPGE. For example, we can choose an incident light with $\boldsymbol{E}(t) = E_0 e^{i\omega_0 t}(1, 0, 0)$ and a magnetic field $\boldsymbol{B}(t) = B_0 e^{i\omega_0 t}(0, 1, 0)$ to induce a pseudo-electric field $\tilde{\boldsymbol{E}}(t) = \tilde{E}_0 e^{i\omega_0 t}(1, -i, 0)$. Thus, using Eq. (31), the MR-induced nonlinear current is $\tilde{\boldsymbol{j}} = -4\tau\beta_0 C_L E_0 \tilde{E}_0 \hat{e}_z$ assuming $n_z = 1$. It should be noted that although the topological invariant C_L appears in this current response, the pseudo-electric field $\tilde{E}_0$ depends on material parameters, not just the fundamental constants, and thus we regard this non-linear current response to be geometric rather than topological.

5 Magnetic-resonance-induced non-linear current response in a microscopic model

The above analytical derivation reveals the non-linear current response induced by MR, in analogy to the regular CPGE. In this section, we will further study the non-linear current response directly from numerical calculations of the Hamiltonian Eq. (1). We emphasize that the purpose of this section is to verify the analytical solutions of the nonlinear current response in the low frequency regime for a more realistic Weyl semimetal model in a certain limit. However, the parameters chosen for the calculations of this model are not realistic, so our calculations *cannot* be directly applied to the realistic material systems. A comment on the additional contribution to the non-linear current response from the remote bands will be provided at the end of this section.

As shown in Appendix 3, the MR-induced non-linear current in the four-band model Eq. (1) can be derived as

$$\tilde{j}_a = \tau\tilde{\eta}_{abc}(0; \omega, -\omega)E_b(\omega)\tilde{E}_c^*(\omega) + \tau\tilde{\eta}_{acb}(0; -\omega, \omega)\tilde{E}_b(\omega)E_c^*(\omega), \tag{32}$$

with

$$\tilde{\eta}_{abc}(0; \omega, -\omega) = i\beta_0 \sum_{nm}\int \frac{d^3k}{2\pi}(\partial_a \varepsilon_{nm}) f_{nm} \frac{\mathcal{A}^b_{nm}\Gamma^c_{mn}}{\varepsilon_{nm}}\delta(\varepsilon_{mn} - \hbar\omega), \tag{33}$$

where $\beta_0 = \pi e^3/h^2$, $\boldsymbol{\mathcal{A}}_{nm}$ is the non-Abelian Berry connection of the unperturbed Hamiltonian H_0, $\boldsymbol{\Gamma} = \boldsymbol{\sigma}\tau_z$, and $\tilde{\boldsymbol{E}}(\omega) = i\hbar\omega\boldsymbol{v}/e$ is the pseudo-electric field induced by the magnetic fluctuation $\boldsymbol{v}$, which comes from the

ferromagnetic resonance by solving the LLG equation in Section 4.

At low energy, the four-band Hamiltonian can be projected to the effective Hamiltonian describing two Weyl points, and the magnetic fluctuation $\boldsymbol{v}$ appears in the form of the chiral gauge field $\boldsymbol{a}$ (see Section 2). In this approximation, we can rewrite $\tilde{\boldsymbol{E}}(\omega)$ as $i\omega\boldsymbol{a}$ following the definition of Eqs. (18) and (33) becomes

$$\tilde{\eta}_{abc}(0;\omega,-\omega) = i\beta_0 \frac{\hbar v_c}{e a_c} \sum_{nm} \int \frac{d^3k}{2\pi} (\partial_a \varepsilon_{nm}) f_{nm} \frac{\mathcal{A}^b_{nm}\Gamma^c_{mn}}{\varepsilon_{nm}} \delta(\varepsilon_{mn} - \hbar\omega), \tag{34}$$

where the pseudo-gauge field $\boldsymbol{a}$ in terms of $\boldsymbol{v}$ is defined in Section 2. Furthermore, Eq. (32) can be recovered to Eq. (20) derived from the effective model for the two Weyl fermions by performing projection to the subspace of the two low-energy bands. This indicates that at the low-energy range, the MR-induced non-linear current trace of this microscopic model should have a quantized value of $2i\beta_0$.

As the magnetization in our model is in the z direction, only an in-plane pseudo-electric field can be induced by the ferromagnetic resonance [38]. We assume the incident light propagates in the z direction and has in-plane electromagnetic fields, so the indices b, c can only be x or y, and $b \neq c$ as the electric fields are along perpendicular directions in CPGE. Furthermore, the four-band model has mirror M_z symmetry which imposes constraints $\tilde{\eta}_{xxy} = \tilde{\eta}_{xyx} = \tilde{\eta}_{yxy} = \tilde{\eta}_{yyx} = 0$, and the in-plane rotational symmetry which imposes $\tilde{\eta}_{zxy} = -\tilde{\eta}_{zyx}$. Therefore, in the following calculations, we focus on the component $\tilde{\eta}_{zxy}$ given by

$$\tilde{\eta}_{zxy} = i\beta_0 \frac{L_2 m}{\sqrt{m^2 - M_0^2}} \sum_{nm} \int \frac{d^3k}{2\pi} (\partial_z \varepsilon_{nm}) f_{nm} \frac{\mathcal{A}^x_{nm}\Gamma^y_{mn}}{\varepsilon_{nm}} \delta(\varepsilon_{mn} - \hbar\omega), \tag{35}$$

where we have used $a_y = \frac{\hbar L_1 K_0}{e L_2 m} v_y$ and $K_0 = \sqrt{m^2 - M_0^2}/L_1$ from Section 2 to derive this result.

Figure 2a shows the energy dispersion of the four-band model along k_z at $k_x = k_y = 0$, in which four bands are labelled by the index $n = 1, ..., 4$ from low to high energies. Two Weyl nodes with opposite charges at opposite k_z are formed by two bands $n = 2$ and 3 around the energy $\varepsilon = 0$. We numerically calculate $\tilde{\eta}_{zxy}$ as a function of $\hbar\omega$, as shown in Fig. 2b. When $\hbar\omega$ is smaller than 0.01 eV (green shaded area), $\tilde{\eta}_{zxy}$ is very close to the quantized value $2i\beta_0$, suggesting that the microscopic model can be simplified as an effective model of two Weyl fermions at the low energy range. At around $\hbar\omega \sim 0.01$ eV, $\tilde{\eta}_{zxy}$ starts to decrease as the effective model of two Weyl fermions is no longer applicable, and thus $\tilde{\eta}_{zxy}$ deviates from quantization. Another reason for the rapid decrease in $\tilde{\eta}_{zxy}$ is that the transitions around the Weyl nodes become only partially activated as $\hbar\omega$ exceeds the energy difference between the middle two bands at $k_z = 0$ ($\Delta\varepsilon \sim 0.04$ eV). Eventually, $\tilde{\eta}_{zxy}$ becomes a constant for $\hbar\omega > 0.06$ eV. Therefore, our numerical result confirms that the MR-induced non-linear current trace between two bands of Weyl nodes can be quantized at the low energy range, where the microscopic model recovers to the effective model of two Weyl fermions, as shown in Section 2. We emphasize that the quantization of $\tilde{\eta}_{zxy}$ does *not* mean that the current $\tilde{j}$ is quantized, as the pseudo-electric field in the response Eq. (32), unlike physical electric field E, is not an externally controlled parameter and depends on specific material parameters.

In our calculation, we have only considered two-band transitions ($2 \to 3$, where 2, 3 label two bands around $\varepsilon = 0$ for two Weyl nodes) and have not included three-band virtual transitions ($2 \to l \to 3$ where $l = 1, 4$ labels the third bands for the three-band contributions to the non-linear current response). It is known that the three-band contribution can play an important role for the CPGE when the third band l is close to the two bands that form Weyl nodes [35], and thus destroys the quantization of CPGE. Similar physics can also occur for the MR-induced non-linear current response here. The ratio between the three-band and two-band contributions can contain the energy separation ratio $\sim \frac{\varepsilon_n - \varepsilon_m}{\varepsilon_n - \varepsilon_l}$ [35], where $n, m = 2, 3$ and $l = 1, 4$. This ratio decays as the energy separation between the third band and two Weyl bands increases. For the chosen model parameters, a typical energy separation between two bands of Weyl nodes is around $0.01 \sim 0.02eV$, below which the linear dispersion of Weyl fermions remains valid. This energy scale is one order smaller than the energy separation between the third band and these two Weyl bands, which is around 0.2 eV. As long as the other bands are far away enough from the two Weyl bands, we expect that the contribution from the three-band transition provides only a small correction.

6 Conclusion and discussion

In conclusion, we demonstrate that a non-linear current response with an electric field and a MR-induced pseudo-electric field can exist in magnetic Weyl semimetals with two Weyl nodes with opposite charges, in contrast to the regular CPGE. The pseudo-electric field can be induced by the magnetic fluctuations from ferromagnetic resonance, which acts like a chiral gauge field that couples oppositely to the lefthanded and righthanded Weyl nodes. Therefore, the realization of MR-induced non-linear current does not require a chiral Weyl semimetal in which the two Weyl nodes are located at different energies. Experimentally, we can consider the electric and magnetic components of an electromagnetic wave acting on magnetic Weyl semimetals. We expect that the direct

coupling between the magnetic field component of electromagnetic wave and electron spin is negligible. The role of the oscillating magnetic field here is to induce a ferromagnetic resonance, a physical phenomenon that has been well observed in experiments. Once the magnetization procession is excited in magnetic Weyl semimetals, it is the exchange coupling between magnetization and electron spin, rather than the Zeeman coupling of magnetic fields, to induce the current response. From Eq. (31), this magnetic-resonance-induced current has the magnitude of $4\tau E_0\tilde{E}_0$, where $\tilde{E}_0 = g_M B_0\gamma_0 M_s/(2ev_f\alpha)$ is the strength of the pseudo-electric field. With typical values of parameters $|g_M M_s| = 0.1$ meV, $B_0 = 10$ G, $\gamma_0 = 1.76\times10^{11}$ C/kg, $v_f = 6.5\times10^5$ m/s, and $|\alpha| = 10^{-5}\sim10^{-2}$ [38], we estimate the magnitude of $\tilde{E}_0$ to be around $1\sim1000$ V/m. Taking a sample thickness of 10 nm, a width of 100 μm, and a typical relaxation time in Weyl semimetals $\tau\sim1$ ps [27], the induced current reaches $1\sim10^3$ nA, which is measurable in experiments. Since any current response at the second-order purely from physical electric fields (E^2 order) will vanish due to the inversion symmetry, this current response from one magnetization and one electric field (EM order) becomes the dominant contribution in centrosymmetric materials.

Appendix 1: Derivation of CPGE in length gauge

In this section, we derive the expression for CPGE current in the length gauge, in which the dipole interaction is treated as [45–47]

$$\hat{H}_E(t) = \int d\boldsymbol{x}\tilde{\psi}^\dagger(\boldsymbol{x})[H_0 + e\boldsymbol{x}\cdot\boldsymbol{E}(t)]\tilde{\psi}(\boldsymbol{x}), \tag{36}$$

where $\boldsymbol{x}$ is the position operator and we define $H_1(t) = e\boldsymbol{x}\cdot\boldsymbol{E}(t)$. H_0 is the unperturbed single-particle Hamiltonian with the eigen-equation

$$H_0(\boldsymbol{k})\psi_{n\boldsymbol{k}}(\boldsymbol{x}) = \varepsilon_{n\boldsymbol{k}}\psi_{n\boldsymbol{k}}(\boldsymbol{x}), \tag{37}$$

where $\varepsilon_{n\boldsymbol{k}}$ is the eigen-energy, $\psi_{n\boldsymbol{k}}(\boldsymbol{x}) = e^{i\boldsymbol{k}\boldsymbol{x}}u_{n\boldsymbol{k}}(\boldsymbol{x})$ is the Bloch wavefunction, and the field operators are expanded as

$$\begin{aligned}\tilde{\psi}(\boldsymbol{x}) &= \sum_n\int d\boldsymbol{k}\psi_{n\boldsymbol{k}}(\boldsymbol{x})\hat{a}_{n\boldsymbol{k}},\\ \tilde{\psi}^\dagger(\boldsymbol{x}) &= \sum_n\int d\boldsymbol{k}\psi^*_{n\boldsymbol{k}}(\boldsymbol{x})\hat{a}^\dagger_{n\boldsymbol{k}},\end{aligned} \tag{38}$$

where $\hat{a}_{n\boldsymbol{k}}$ and $\hat{a}^\dagger_{n\boldsymbol{k}}$ are the annihilation and creation operators, and the orthogonality of the Bloch states as well as the anticommutation relation read

$$\langle\psi_{n\boldsymbol{k}}|\psi_{m\boldsymbol{k}'}\rangle = \int d\boldsymbol{x}\psi^*_{n\boldsymbol{k}}(\boldsymbol{x})\psi_{m\boldsymbol{k}'}(\boldsymbol{x}) = \delta_{nm}\delta(\boldsymbol{k}-\boldsymbol{k}'), \tag{39}$$

$$\left\{\hat{a}_{n\boldsymbol{k}}, \hat{a}^\dagger_{m\boldsymbol{k}'}\right\} = \delta_{nm}\delta(\boldsymbol{k}-\boldsymbol{k}'). \tag{40}$$

Next, we solve the equation of motion of the density operator [48]

$$\frac{\partial\rho_{nm}(t)}{\partial t} = -\frac{i}{\hbar}[H(t),\rho(t)]_{nm} - \frac{\rho_{nm}(t)-\rho^{(0)}_{nm}}{\tau}, \tag{41}$$

where $\rho^{(0)}_{nm} = f_n\delta_{nm}$ is the initial density operator with the Fermi factor f_n of band n, and the latter term is the phenomenological term with the relaxation time τ which describes the scattering processes of electrons [48]. We expand the density operator in powers of $\boldsymbol{E}$ as

$$\rho(t) = \rho^{(0)} + \rho^{(1)}(t) + \rho^{(2)}(t) + \cdots, \tag{42}$$

and the equation of motion for the i-th order is then

$$\frac{\partial\rho^{(i)}_{nm}(t)}{\partial t} = -\frac{i}{\hbar}\left[H_0,\rho^{(i)}(t)\right]_{nm} - \frac{i}{\hbar}\left[H_1(t),\rho^{(i-1)}(t)\right]_{nm} - \frac{\rho^{(i)}_{nm}(t)}{\tau_i}. \tag{43}$$

The matrix element of the position operator $\boldsymbol{x}$ is [46, 47, 49]

$$\langle n\boldsymbol{k}|\boldsymbol{x}|m\boldsymbol{k}'\rangle = (i\partial_{\boldsymbol{k}} + \boldsymbol{\mathcal{A}}_{nm})\delta_{nm}\delta(\boldsymbol{k}-\boldsymbol{k}') + \boldsymbol{\mathcal{A}}_{nm}(1-\delta_{nm})\delta(\boldsymbol{k}-\boldsymbol{k}'), \tag{44}$$

where $\boldsymbol{\mathcal{A}}_{nm} = \langle n|i\partial_{\boldsymbol{k}}|m\rangle$ is the Berry connection. We define the covariant derivative as follows [46]

$$\boldsymbol{D}_{nm,\boldsymbol{k}} = \delta_{nm}\partial_{\boldsymbol{k}} - i\boldsymbol{\mathcal{A}}_{nm}, \tag{45}$$

so for an operator $\mathcal{O}_{nm}(k)$, the commutator with H_1 is

$$[H_1(t),\mathcal{O}(k)]_{nm} = e\boldsymbol{E}(t)[\boldsymbol{x},\mathcal{O}(k)]_{nm} = ieE^b(t)\left[D_{k^b},\mathcal{O}(k)\right]_{nm}, \tag{46}$$

with the summation over index b, and

$$\left[D_{k^b},\mathcal{O}(k)\right]_{nm} = \partial_b\mathcal{O}_{nm}(k) - i\left[\mathcal{A}^b,\mathcal{O}(k)\right]_{nm}, \tag{47}$$

where $\partial_b = \partial/\partial k^b$. At the first order, we write $E^b(t) = E^b_\beta e^{-i\omega_\beta t}$ with summation over the frequency index β, and the equation of motion reads

$$\begin{aligned}\frac{\partial\rho^{(1)}_{nm}(t)}{\partial t} &= -\frac{i}{\hbar}\left[H_0,\rho^{(1)}(t)\right]_{nm} - \frac{i}{\hbar}\left[H_1(t),\rho^{(0)}\right]_{nm} - \frac{\rho^{(1)}_{nm}(t)}{\tau_1}\\ &= -\frac{i}{\hbar}\varepsilon_{nm}\rho^{(1)}_{nm}(t) + \frac{e}{\hbar}E^b_\beta e^{-i\omega_\beta t}\left[D^b,\rho^{(0)}\right]_{nm} - \frac{\rho^{(1)}_{nm}(t)}{\tau_1},\end{aligned} \tag{48}$$

where $\varepsilon_{nm} = \varepsilon_n - \varepsilon_m$ with ε_n being the eigen-energy of the unperturbed Hamiltonian H_0, and we replace D_{k^b} with D^b. By writing $\rho^{(1)}_{nm}(t) = \tilde{p}^{(1)}_{nm}e^{-i\tilde{\omega}_{1,nm}t}$ with $\tilde{\omega}_{1,nm} = \omega_{nm} - i/\tau_1$ and $\omega_{nm} = \varepsilon_{nm}/\hbar$, we obtain

$$\frac{\partial \tilde{p}^{(1)}_{nm}}{\partial t} = \frac{e}{\hbar} E^b_\beta e^{-i(\omega_\beta - \tilde{\omega}_{1,nm})t} \left[D^b, \rho^{(0)}\right]_{nm},$$
$$\tilde{p}^{(1)}_{nm} = \frac{e E^b_\beta e^{-i(\omega_\beta - \tilde{\omega}_{1,nm})t} \left[D^b, \rho^{(0)}\right]_{nm}}{i\hbar(\tilde{\omega}_{1,nm} - \omega_\beta)}. \tag{49}$$

Thus, the first-order term of the density operator is

$$\rho^{(1)}_{nm}(t) = \frac{e\left[D^b, \rho^{(0)}\right]_{nm}}{i\hbar(\omega_{nm} - \omega_\beta - i/\tau_1)} E^b_\beta e^{-i\omega_\beta t}, \tag{50}$$

where

$$\left[D^b, \rho^{(0)}\right]_{nm} = \partial_b f_n \delta_{nm} - i f_{mn} \mathcal{A}^b_{nm}. \tag{51}$$

At the second order, we have

$$\rho^{(2)}_{nm}(t) = -\frac{e^2 \Lambda^{(2)}_{nm}}{\hbar^2(\omega_{nm} - \omega_\Sigma - i/\tau_2)} E^b_\beta E^c_\gamma e^{-i\omega_\Sigma t}, \tag{54}$$

where $\omega_\Sigma = \omega_\beta + \omega_\gamma$ and

$$\Lambda^{(2)}_{nm} = \left[D^c, \frac{\left[D^b, \rho^{(0)}\right]}{\tilde{\omega}_1 - \omega_\beta}\right]_{nm}. \tag{55}$$

We then separate the second-order density operator $\rho^{(2)}_{nm}(t)$ in Eq. (54) into the diagonal (intraband) $\rho^{(2)}_{nn}(t)$ and off-diagonal (interband) $(1-\delta_{nm})\rho^{(2)}_{nm}(t)$ parts [47]. The intraband contribution reads

$$\rho^{(2)}_{nn}(t) = \frac{e^2 \Lambda^{(2)}_{nn}}{\hbar^2(\omega_\Sigma + i/\tau_2)} E^b_\beta E^c_\gamma e^{-i\omega_\Sigma t}, \tag{56}$$

where

$$\begin{aligned}
\Lambda^{(2)}_{nn} &= \left[D^c, \frac{\left[D^b, \rho^{(0)}\right]}{\tilde{\omega}_1 - \omega_\beta}\right]_{nn} \\
&= -\partial_c \frac{\left[D^b, \rho^{(0)}\right]_{nn}}{\omega_\beta + i/\tau_1} - i \sum_m \left(\mathcal{A}^c_{nm} \frac{\left[D^b, \rho^{(0)}\right]_{mn}}{\tilde{\omega}_{1,mn} - \omega_\beta} - \frac{\left[D^b, \rho^{(0)}\right]_{nm}}{\tilde{\omega}_{1,nm} - \omega_\beta} \mathcal{A}^c_{mn} \right) \\
&= -\frac{\partial_b \partial_c f_n}{\omega_\beta + i/\tau_1} - \sum_m \left(\frac{f_{nm} \mathcal{A}^b_{mn} \mathcal{A}^c_{nm}}{\tilde{\omega}_{1,mn} - \omega_\beta} - \frac{f_{mn} \mathcal{A}^b_{nm} \mathcal{A}^c_{mn}}{\tilde{\omega}_{1,nm} - \omega_\beta} \right).
\end{aligned} \tag{57}$$

$$\frac{\partial \rho^{(2)}_{nm}(t)}{\partial t} = -\frac{i}{\hbar}\left[H_0, \rho^{(2)}(t)\right]_{nm} - \frac{i}{\hbar}\left[H_1(t), \rho^{(1)}\right]_{nm} - \frac{\rho^{(2)}_{nm}(t)}{\tau_2}. \tag{52}$$

By writing $E^c(t) = E^c_\gamma e^{-i\omega_\gamma t}$, $\rho^{(2)}_{nm}(t) = \tilde{p}^{(2)}_{nm} e^{-i\tilde{\omega}_{2,nm} t}$ with $\tilde{\omega}_{2,nm} = \omega_{nm} - i/\tau_2$, we get

$$\frac{\partial \tilde{p}^{(2)}_{nm}}{\partial t} = \frac{e}{\hbar} E^c_\gamma e^{-i(\omega_\gamma - \tilde{\omega}_{2,nm})t} \left[D^c, \rho^{(1)}(t)\right]_{nm}. \tag{53}$$

We then use the expression for $\rho^{(1)}_{nm}(t)$ in Eq. (50) and integrate out t to obtain

The corresponding current is

$$\begin{aligned}
j^a_{\text{intra}}(t) &= -\frac{e^3}{\hbar^2 \omega_\Sigma} \sum_n \int_k v^a_{nn} \Lambda^{(2)}_{nn} E^b_\beta E^c_\gamma e^{-i\omega_\Sigma t} \\
&= \frac{e^3}{\hbar^2 \omega_\Sigma} \sum_{nm} \int_k v^a_{nn} \left(\frac{f_{nm} \mathcal{A}^b_{mn} \mathcal{A}^c_{nm}}{\tilde{\omega}_{1,mn} - \omega_\beta} - \frac{f_{mn} \mathcal{A}^b_{nm} \mathcal{A}^c_{mn}}{\tilde{\omega}_{1,nm} - \omega_\beta} \right) E^b_\beta E^c_\gamma e^{-i\omega_\Sigma t} \\
&= \frac{e^3}{\hbar^2 \omega_\Sigma} \sum_{nm} \int_k \left(\frac{\Delta^a_{nm} f_{nm} \mathcal{A}^b_{mn} \mathcal{A}^c_{nm}}{\tilde{\omega}_{1,mn} - \omega_\beta} \right) E^b_\beta E^c_\gamma e^{-i\omega_\Sigma t},
\end{aligned} \tag{58}$$

where $\Delta^a_{nm} = v^a_{nn} - v^a_{mm}$ and we take $\tau_2 \to \infty$ and $\partial_k f_n = 0$. We then symmetrize the indices $b\beta \leftrightarrow c\gamma$, $\boldsymbol{k} \leftrightarrow -\boldsymbol{k}$, and $n \leftrightarrow m$ to get

$$\begin{aligned}
j^a_{\text{intra}}(t) &= \frac{e^3}{2\hbar^2 \omega_\Sigma} \sum_{nm} \int_k \Delta^a_{nm} f_{nm} \left(\frac{\mathcal{A}^b_{mn} \mathcal{A}^c_{nm}}{\tilde{\omega}_{1,mn} - \omega_\beta} + \frac{\mathcal{A}^c_{mn} \mathcal{A}^b_{nm}}{\tilde{\omega}_{1,mn} - \omega_\gamma} \right) E^b_\beta E^c_\gamma e^{-i\omega_\Sigma t} \\
&= \frac{e^3}{4\hbar^2 \omega_\Sigma} \sum_{nm} \int_k \Delta^a_{nm} f_{nm} (\mathcal{A}^b_{mn} \mathcal{A}^c_{nm} - \mathcal{A}^c_{mn} \mathcal{A}^b_{nm}) \left(\frac{1}{\tilde{\omega}_{1,mn} - \omega_\beta} - \frac{1}{\tilde{\omega}_{1,mn} - \omega_\gamma} \right) E^b_\beta E^c_\gamma e^{-i\omega_\Sigma t} \\
&= \frac{e^3}{8\hbar^2 \omega_\Sigma} \sum_{nm} \int_k \Delta^a_{nm} f_{nm} (\mathcal{A}^b_{mn} \mathcal{A}^c_{nm} - \mathcal{A}^c_{mn} \mathcal{A}^b_{nm}) \\
&\quad \times \left(\frac{1}{\tilde{\omega}_{1,mn} - \omega_\beta} + \frac{1}{\tilde{\omega}_{1,mn} + \omega_\beta} - \frac{1}{\tilde{\omega}_{1,mn} - \omega_\gamma} - \frac{1}{\tilde{\omega}_{1,mn} + \omega_\gamma} \right) E^b_\beta E^c_\gamma e^{-i\omega_\Sigma t}.
\end{aligned} \tag{59}$$

By assuming $1/\tau_1$ is very small, i.e. $\tau_1 \to \infty$, we can apply the following identity

$$\frac{1}{\tilde{\omega}_{1,mn} - \omega_\beta} = \frac{1}{\omega_{mn} - \omega_\beta - i/\tau_1} = \frac{P}{\omega_{mn} - \omega_\beta} + i\pi\delta(\omega_{mn} - \omega_\beta), \tag{60}$$

where P denotes a Cauchy principle value. The imaginary part of the current is called the injection current or the circular photocurrent [47], which reads

$$j^a_{\text{injection}}(t) = [j^a_{\text{intra}}(t)]_{\text{Im}} = \frac{i\pi e^3}{8\hbar^2\omega_\Sigma} \sum_{nm} \int_k \Delta^a_{nm} f_{nm} (\mathcal{A}^b_{mn}\mathcal{A}^c_{nm} - \mathcal{A}^c_{mn}\mathcal{A}^b_{nm}) \times \left[\delta(\omega_{mn} - \omega_\beta) - \delta(\omega_{mn} + \omega_\beta) - \delta(\omega_{mn} - \omega_\gamma) + \delta(\omega_{mn} + \omega_\gamma)\right] E^b_\beta E^c_\gamma e^{-i\omega_\Sigma t}. \tag{61}$$

We then take the time derivative of the current

$$\frac{d j^a_{\text{injection}}(t)}{dt} = -i\omega_\Sigma \times [j^a_{\text{intra}}(t)]_{\text{Im}} = \eta_{abc}(\omega_\Sigma; \omega_\beta, \omega_\gamma) E^b_\beta E^c_\gamma e^{-i\omega_\Sigma t}, \tag{62}$$

where

$$\eta_{abc}(\omega_\Sigma; \omega_\beta, \omega_\gamma) = -\frac{i\pi e^3}{8\hbar^2} \sum_{nm} \int_k \Delta^a_{nm} f_{nm} \Omega^{bc}_{mn} \times \left[\delta(\omega_{mn} - \omega_\beta) - \delta(\omega_{mn} + \omega_\beta) - \delta(\omega_{mn} - \omega_\gamma) + \delta(\omega_{mn} + \omega_\gamma)\right]. \tag{63}$$

If we consider a monochromatic field $\boldsymbol{E}(t) = \boldsymbol{E}(\omega)e^{-i\omega t} + \boldsymbol{E}(-\omega)e^{i\omega t}$, the injection current with $\omega_\Sigma = 0$ is

$$\frac{d j^a_{\text{injection}}(t)}{dt} = 2\eta_{abc}(0; -\omega, \omega) E^b(\omega) E^c(-\omega), \tag{64}$$

with

$$\eta_{abc}(0; -\omega, \omega) = -\frac{i\pi e^3}{2\hbar^2} \sum_{nm} \int_k \Delta^a_{nm} f_{nm} \Omega^{bc}_{mn} \delta(\omega_{mn} - \omega). \tag{65}$$

The same result can be also derived from the velocity gauge, as shown in Appendix 2. We can rewrite Eq. (64) as [27, 34]

$$j^a_{\text{injection}} = \tau\beta_{ab}(\omega)[\boldsymbol{E}(\omega) \times \boldsymbol{E}^*(\omega)]^b, \tag{66}$$

with

$$\beta_{ab}(\omega) = \frac{\pi e^3}{\hbar^2} \sum_{nm} \int \frac{d^3k}{(2\pi)^3} (\partial_a \varepsilon_{nm}) f_{nm} R^b_{nm} \delta(\varepsilon_{mn} - \hbar\omega), \tag{67}$$

where τ is the lifetime and $\boldsymbol{R}_{nm} = (\boldsymbol{\mathcal{A}}_{nm} \times \boldsymbol{\mathcal{A}}_{mn})$. We can see that this current can be generated by a circularly polarized light, but not a linearly polarized light, as $\boldsymbol{E} \times \boldsymbol{E}^*$ requires the electric fields to be along perpendicular directions, thus the name "circular photogalvanic effect". Furthermore, the current switches direction when the polarization changes from lefthanded to righthanded. The CPGE trace $\beta(\omega)$ reads

$$\beta(\omega) = \text{Tr}[\beta_{ab}(\omega)] = \frac{\pi e^3}{\hbar^2} \sum_{nm} \int \frac{d^3k}{(2\pi)^3} (\partial_a \varepsilon_{nm}) f_{nm} R^a_{nm} \delta(\varepsilon_{mn} - \hbar\omega) = \frac{e^3}{2\hbar^2} \sum_{nm} \oint d\boldsymbol{S}_{nm} \cdot \boldsymbol{R}_{nm}, \tag{68}$$

where $\boldsymbol{S}_{nm}$ is a closed surface in the momentum space. For a two-fold Weyl node with band index $n = 1, 2$ and Fermi energy across at the Weyl node, we use the relation $\boldsymbol{\Omega}_{nm} = i\sum_{m\neq n} \boldsymbol{R}_{nm}$ [34], and Eq. (68) becomes

$$\beta(\omega) = i\frac{e^3}{2h^2} \oint d\boldsymbol{S} \cdot \boldsymbol{\Omega}_1 = i\beta_0 C, \tag{69}$$

where $C = \frac{1}{2\pi} \oint \boldsymbol{S} \cdot \boldsymbol{\Omega}$ is the Chern number and $\beta_0 = \pi e^3/h^2$. Therefore, the CPGE trace $\beta(\omega)$ is quantized for a Weyl node as proportional to its associated topological charge, and the CPGE current can be written as

$$\boldsymbol{j} = i\tau\beta_0 C\left[\boldsymbol{E}(\omega) \times \boldsymbol{E}^*(\omega)\right]. \tag{70}$$

For a two-band Weyl semimetal with mirror symmetry, there are two Weyl nodes with opposite topological charges $C_L = 1$ and $C_R = -1$ sitting at the same energy (Fig. 1a). When the Fermi energy is at the Weyl node, the CPGE trace for the two Weyl nodes are $i\beta_0 C_L$ and $i\beta_0 C_R$. The CPGE currents from the left and right Weyl nodes are $\boldsymbol{j}_L = i\tau\beta_0 C[\boldsymbol{E}(\omega) \times \boldsymbol{E}^*(\omega)]$ and $\boldsymbol{j}_R = -i\tau\beta_0 C[\boldsymbol{E}(\omega) \times \boldsymbol{E}^*(\omega)]$, so the total CPGE current vanishes. If we consider a chiral Weyl semimetal in which the inversion and all mirror symmetries are broken (Fig. 1b), the left and right Weyl nodes are located at different energies ε_L and ε_R (measured from the Fermi energy E_f), respectively. Then in the frequency window $2|\varepsilon_R| < \hbar\omega < 2|\varepsilon_L|$, the transition near the left Weyl node is forbidden due to Pauli blocking, and thus, the only contribution to the CPGE current comes from the right Weyl node $\boldsymbol{j}_R = -i\tau\beta_0 C[\boldsymbol{E}(\omega) \times \boldsymbol{E}^*(\omega)]$ [27]. Therefore, the quantized CPGE can be realized under such conditions. The CPGE has recently been observed in chiral Weyl semimetals RhSi [29, 31] and CoSi [30].

Appendix 2: Derivation of CPGE in velocity gauge

In this section, we derive the CPGE in the velocity gauge [46, 49, 50]. The dipole interaction is written as

$$H_0\left(\boldsymbol{k}+\frac{e}{\hbar}\boldsymbol{A}(t)\right)\approx H_0(\boldsymbol{k})+\boldsymbol{A}(t)\cdot\boldsymbol{J}=H_0(\boldsymbol{k})+H_1, \tag{71}$$

where $\boldsymbol{J}=\frac{e}{\hbar}\frac{\partial H_0}{\partial \boldsymbol{k}}$ is the current operator. Using the expressions in Appendix 1, we obtain the second-quantized Hamiltonian

$$\begin{aligned}\hat{H}_0&=\int d\boldsymbol{x}\tilde{\psi}^{\dagger}(\boldsymbol{x})H_0\tilde{\psi}(\boldsymbol{x})\\&=\sum_{nn'}\int d\boldsymbol{k}d\boldsymbol{k}'d\boldsymbol{x}\psi^{*}_{n\boldsymbol{k}}(\boldsymbol{x})\hat{a}^{\dagger}_{n\boldsymbol{k}}\varepsilon_{n'\boldsymbol{k}'}\psi_{n'\boldsymbol{k}'}(\boldsymbol{x})\hat{a}_{n'\boldsymbol{k}'}\\&=\sum_{n}\int d\boldsymbol{k}\varepsilon_{n\boldsymbol{k}}\hat{a}^{\dagger}_{n\boldsymbol{k}}\hat{a}_{n\boldsymbol{k}},\end{aligned} \tag{72}$$

$$\begin{aligned}\hat{H}_1&=\int d\boldsymbol{x}\tilde{\psi}^{\dagger}(\boldsymbol{x})\boldsymbol{A}(t)\cdot\boldsymbol{J}\tilde{\psi}(\boldsymbol{x})\\&=\sum_{nn'}\int d\boldsymbol{k}d\boldsymbol{k}'\hat{a}^{\dagger}_{n\boldsymbol{k}}\hat{a}_{n'\boldsymbol{k}'}\int d\boldsymbol{x}d\boldsymbol{q}e^{i(-\boldsymbol{k}+\boldsymbol{q}+\boldsymbol{k}')\boldsymbol{x}}u^{*}_{n\boldsymbol{k}}[\boldsymbol{A}(\boldsymbol{q},t)\cdot\boldsymbol{J}]u_{n'\boldsymbol{k}'}(\boldsymbol{x})\\&=\sum_{nn'}\int d\boldsymbol{k}d\boldsymbol{k}'\hat{a}^{\dagger}_{n\boldsymbol{k}}\hat{a}_{n'\boldsymbol{k}'}\int d\boldsymbol{q}\delta(-\boldsymbol{k}+\boldsymbol{q}+\boldsymbol{k}')\langle u_{n\boldsymbol{k}}|\boldsymbol{A}(\boldsymbol{q},t)\cdot\boldsymbol{J}|u_{n'\boldsymbol{k}'}\rangle\\&=\sum_{nn'}\int d\boldsymbol{k}d\boldsymbol{k}'\hat{a}^{\dagger}_{n\boldsymbol{k}}\hat{a}_{n'\boldsymbol{k}'}\langle u_{n\boldsymbol{k}}|\boldsymbol{A}(\boldsymbol{k}-\boldsymbol{k}',t)\cdot\boldsymbol{J}|u_{n'\boldsymbol{k}'}\rangle.\end{aligned} \tag{73}$$

We assume the photon momentum is zero $\boldsymbol{q}\approx 0$, i.e. $\boldsymbol{k}-\boldsymbol{k}'\approx 0$, as the momentum of light $\boldsymbol{q}$ is much smaller than that of electrons $\boldsymbol{k}$, so the Hamiltonian is as follows

$$\hat{H}=\sum_{n}\int d\boldsymbol{k}\varepsilon_{n\boldsymbol{k}}\hat{a}^{\dagger}_{n\boldsymbol{k}}\hat{a}_{n\boldsymbol{k}}+\sum_{nn'}\int d\boldsymbol{k}\hat{a}^{\dagger}_{n\boldsymbol{k}}\hat{a}_{n'\boldsymbol{k}}\boldsymbol{A}(t)\cdot\boldsymbol{J}_{nn'\boldsymbol{k}}, \tag{74}$$

where $\boldsymbol{J}_{nn'\boldsymbol{k}}=\langle u_{n\boldsymbol{k}}|\boldsymbol{J}|u_{n'\boldsymbol{k}}\rangle$. The Heisenberg equations of motion for the creation and annihilation operators are

$$\begin{aligned}\frac{\partial\hat{a}_{n\boldsymbol{k}}}{\partial t}&=-\frac{i}{\hbar}\left[\hat{H},\hat{a}_{n\boldsymbol{k}}\right]\\&=\frac{i}{\hbar}\left(\varepsilon_{n\boldsymbol{k}}\hat{a}_{n\boldsymbol{k}}+\sum_{n'}\boldsymbol{A}(t)\cdot\boldsymbol{J}_{nn'\boldsymbol{k}}\hat{a}_{n'\boldsymbol{k}}\right),\\\frac{\partial\hat{a}^{\dagger}_{n\boldsymbol{k}}}{\partial t}&=-\frac{i}{\hbar}\left[\hat{H},\hat{a}^{\dagger}_{n\boldsymbol{k}}\right]\\&=-\frac{i}{\hbar}\left(\varepsilon_{n\boldsymbol{k}}\hat{a}^{\dagger}_{n\boldsymbol{k}}+\sum_{n'}\boldsymbol{A}(t)\cdot\boldsymbol{J}_{n'n\boldsymbol{k}}\hat{a}^{\dagger}_{n'\boldsymbol{k}}\right).\end{aligned} \tag{75}$$

The density matrix is $\rho_{nm,\boldsymbol{k}}=\langle\hat{a}^{\dagger}_{m\boldsymbol{k}}\hat{a}_{n\boldsymbol{k}}\rangle$, so the optical Bloch equation for the density matrix writes

$$\begin{aligned}\frac{\partial\rho_{nm}(t)}{\partial t}&=-\frac{i}{\hbar}\varepsilon_{nm}\rho_{nm}(t)-\frac{i}{\hbar}\sum_{n'}[\boldsymbol{A}(t)\cdot\boldsymbol{J}_{n'n}\rho_{n'm}(t)-\boldsymbol{A}(t)\cdot\boldsymbol{J}_{mn'}\rho_{nn'}(t)]\\&\quad-\frac{\rho_{nm}(t)}{\tau}.\end{aligned} \tag{76}$$

Next we expand the density operator in powers of $\boldsymbol{E}$ as in Eq. (42) and the zeroth-order term is $\rho^{(0)}_{nm}=f_n\delta_{nm}$. At the first order,

$$\begin{aligned}\frac{\partial\rho^{(1)}_{nm}(t)}{\partial t}&=-\frac{i}{\hbar}\varepsilon_{nm}\rho^{(1)}_{nm}(t)-\frac{i}{\hbar}\sum_{n'}\left[\boldsymbol{A}(t)\cdot\boldsymbol{J}_{n'n}\rho^{(0)}_{n'm}(t)-\boldsymbol{A}(t)\cdot\boldsymbol{J}_{mn'}\rho^{(0)}_{nn'}(t)\right]-\frac{\rho^{(1)}_{nm}(t)}{\tau_1}\\&=-\frac{i}{\hbar}\varepsilon_{nm}\rho^{(1)}_{nm}(t)-\frac{i}{\hbar}f_{mn}A^{b}(t)J^{b}_{mn}-\frac{\rho^{(1)}_{nm}(t)}{\tau_1}.\end{aligned} \tag{77}$$

Let $\rho^{(1)}_{nm}(t)=\tilde{p}^{(1)}_{nm}e^{-i\tilde{\omega}_{1,nm}t}$ with $\tilde{\omega}_{1,nm}=\varepsilon_{nm}/\hbar-i/\tau_1$, and $A^{b}(t)=\int\frac{d\omega_\beta}{2\pi}A^{b}(\omega_\beta)e^{-i\omega_\beta t}$, we then obtain

$$\begin{aligned}\frac{\partial\tilde{p}^{(1)}_{nm}}{\partial t}&=-\frac{i}{\hbar}\int\frac{d\omega_\beta}{2\pi}f_{mn}A^{b}(\omega_\beta)J^{b}_{mn}e^{i(\tilde{\omega}_{1,nm}-\omega_\beta)t},\\\tilde{p}^{(1)}_{nm}&=-\frac{i}{\hbar}\int\frac{d\omega_\beta}{2\pi}f_{mn}A^{b}(\omega_\beta)J^{b}_{mn}\frac{e^{i(\tilde{\omega}_{1,nm}-\omega_\beta)t}}{i(\tilde{\omega}_{1,nm}-\omega_\beta)},\end{aligned} \tag{78}$$

so the first-order density operator is

$$\begin{aligned}\rho^{(1)}_{nm}(\omega)&=\int dt\rho^{(1)}_{nm}(t)e^{i\omega t}\\&=-\frac{i}{\hbar}\int\frac{d\omega_\beta}{2\pi}f_{mn}A^{b}(\omega_\beta)J^{b}_{mn}\int dt\frac{e^{i(\omega-\omega_\beta)t}}{i(\tilde{\omega}_{1,nm}-\omega_\beta)}\\&=-\frac{i}{\hbar}\int\frac{d\omega_\beta}{2\pi}f_{mn}A^{b}(\omega_\beta)J^{b}_{mn}\frac{\delta(\omega-\omega_\beta)}{i(\tilde{\omega}_{1,nm}-\omega_\beta)}\\&=\frac{f_{nm}A^{b}(\omega)J^{b}_{mn}}{\hbar(\tilde{\omega}_{1,nm}-\omega)}.\end{aligned} \tag{79}$$

At the second order, the diagonal part (intraband) of the density operator reads

$$\frac{\partial\rho^{(2)}_{nn}(t)}{\partial t}=-\frac{i}{\hbar}\sum_{m}\left[\boldsymbol{A}(t)\cdot\boldsymbol{J}_{mn}\rho^{(1)}_{mn}(t)-\boldsymbol{A}(t)\cdot\boldsymbol{J}_{nm}\rho^{(1)}_{nm}(t)\right]-\frac{\rho^{(2)}_{nn}(t)}{\tau_2}. \tag{80}$$

Let $\rho^{(2)}_{nn}=e^{-t/\tau_2}\tilde{p}^{(2)}_{nn}$,

$$\begin{aligned}\frac{\partial\tilde{p}^{(2)}_{nn}}{\partial t}&=-\frac{i}{\hbar}\sum_{m}A^{c}(t)[J^{c}_{mn}\rho^{(1)}_{mn}(t)-J^{c}_{nm}\rho^{(1)}_{nm}(t)]e^{t/\tau_2}\\&=-\frac{i}{\hbar}\sum_{m}\int\frac{d\omega_\beta d\omega_\gamma}{(2\pi)^2}A^{c}(\omega_\gamma)[J^{c}_{mn}\rho^{(1)}_{mn}(\omega_\beta)-J^{c}_{nm}\rho^{(1)}_{nm}(\omega_\beta)]e^{-i(\omega_\beta+\omega_\gamma+i/\tau_2)t},\\\tilde{p}^{(2)}_{nn}&=\sum_{m}\int\frac{d\omega_\beta d\omega_\gamma}{(2\pi)^2}A^{c}(\omega_\gamma)[J^{c}_{mn}\rho^{(1)}_{mn}(\omega_\beta)-J^{c}_{nm}\rho^{(1)}_{nm}(\omega_\beta)]\frac{e^{-i(\omega_\beta+\omega_\gamma+i/\tau_2)t}}{\hbar(\omega_\beta+\omega_\gamma+i/\tau_2)}.\end{aligned} \tag{81}$$

Thus, the second-order intraband density operator writes

$$\begin{aligned}\rho^{(2)}_{nn}(\omega) &= \int dt \tilde{p}^{(2)}_{nn} e^{i(\omega+i/\tau_2)t} \\ &= \sum_m \int \frac{d\omega_\beta d\omega_\gamma}{(2\pi)^2} A^c(\omega_\gamma)[J^c_{mn}\rho^{(1)}_{mn}(\omega_\beta) - J^c_{nm}\rho^{(1)}_{nm}(\omega_\beta)] \frac{\delta(\omega_\beta+\omega_\gamma-\omega)}{\hbar(\omega_\beta+\omega_\gamma+i/\tau_2)} \\ &= \frac{1}{\hbar(\omega+i/\tau_2)} \sum_m \int \frac{d\omega_\beta d\omega_\gamma}{(2\pi)^2} A^c(\omega_\gamma)[J^c_{mn}\rho^{(1)}_{mn}(\omega_\beta) - J^c_{nm}\rho^{(1)}_{nm}(\omega_\beta)]\delta(\omega_\beta+\omega_\gamma-\omega).\end{aligned} \tag{82}$$

We then use the expression for $\rho^{(1)}_{nm}$ and $A^b_\beta = A^b(\omega_\beta)$, $A^c_\gamma = A^c(\omega_\gamma)$, and $\omega_\Sigma = \omega_\beta + \omega_\gamma$ to get

$$\rho^{(2)}_{nn}(\omega_\Sigma) = \frac{1}{\hbar(\omega_\Sigma+i/\tau_2)} \sum_m A^b_\beta A^c_\gamma \left[\frac{f_{mn}J^b_{mn}J^c_{nm}}{\hbar(\tilde{\omega}_{1,mn}-\omega_\beta)} - \frac{f_{nm}J^b_{nm}J^c_{mn}}{\hbar(\tilde{\omega}_{1,nm}-\omega_\beta)} \right], \tag{83}$$

with the summation over indices β and γ implied. The corresponding current is as follows

$$\begin{aligned} j^a_{\text{intra}}(t) &= e\sum_n \int_k v^a_{nn}\rho^{(2)}_{nn}(\omega_\Sigma)e^{-i\omega_\Sigma t} \\ &= \frac{e}{\hbar^2}\sum_{nm}\int_k v^a_{nn}\left[\frac{f_{mn}J^b_{mn}J^c_{nm}}{\tilde{\omega}_{1,mn}-\omega_\beta} - \frac{f_{nm}J^b_{nm}J^c_{mn}}{\tilde{\omega}_{1,nm}-\omega_\beta}\right]\frac{A^b_\beta A^c_\gamma e^{-i\omega_\Sigma t}}{\omega_\Sigma+i/\tau_2} \\ &= \frac{e}{\hbar^2\omega_\Sigma}\sum_{nm}\int_k \frac{\Delta^a_{nm}f_{mn}J^b_{mn}J^c_{nm}}{\tilde{\omega}_{1,mn}-\omega_\beta}A^b_\beta A^c_\gamma e^{-i\omega_\Sigma t}, \end{aligned} \tag{84}$$

where $\Delta^a_{nm} = v^a_{nn} - v^a_{mm}$ is the velocity shift. We replace $A^b(\omega)$ with $E^b(\omega)/i\omega$ [49] and $J^b_{nm} = \frac{ie}{\hbar}\varepsilon_{nm}\mathcal{A}^b_{nm}$ and obtain

$$j^a_{\text{intra}}(t) = \frac{e^3}{\hbar^2\omega_\Sigma}\sum_{nm}\int_k \frac{\Delta^a_{nm}f_{mn}\mathcal{A}^b_{mn}\mathcal{A}^c_{nm}}{\tilde{\omega}_{1,mn}-\omega_\beta}\frac{\varepsilon^2_{nm}E^b_\beta E^c_\gamma}{\hbar^2\omega_\beta\omega_\gamma}e^{-i\omega_\Sigma t}. \tag{85}$$

We then take the imaginary part of the current using the identity Eq. (60) and symmetrize all the indices to get

$$\begin{aligned} j^a_{\text{lm}}(t) = \frac{i\pi e^3}{8\hbar^2\omega_\Sigma}\sum_{nm}\int_k \Delta^a_{nm}f_{nm}(\mathcal{A}^b_{mn}\mathcal{A}^c_{nm} - \mathcal{A}^c_{mn}\mathcal{A}^b_{nm})\frac{\varepsilon^2_{nm}E^b_\beta E^c_\gamma}{\hbar^2\omega_\beta\omega_\gamma}e^{-i\omega_\Sigma t} \\ \times\left[\delta(\omega_{mn}-\omega_\beta) - \delta(\omega_{mn}+\omega_\beta) - \delta(\omega_{mn}-\omega_\gamma) + \delta(\omega_{mn}+\omega_\gamma)\right]. \end{aligned} \tag{86}$$

The time derivative of the above current reads

$$\begin{aligned} \frac{dj^a_{\text{lm}}(t)}{dt} &= \frac{\pi e^3}{8\hbar^2}\sum_{nm}\int_k \Delta^a_{nm}f_{nm}(\mathcal{A}^b_{mn}\mathcal{A}^c_{nm} - \mathcal{A}^c_{mn}\mathcal{A}^b_{nm})\frac{\varepsilon^2_{nm}E^b_\beta E^c_\gamma}{\hbar^2\omega_\beta\omega_\gamma}e^{-i\omega_\Sigma t} \\ &\times\left[\delta(\omega_{mn}-\omega_\beta) - \delta(\omega_{mn}+\omega_\beta) - \delta(\omega_{mn}-\omega_\gamma) + \delta(\omega_{mn}+\omega_\gamma)\right] \\ &= \eta_{abc}(\omega_\Sigma;\omega_\beta,\omega_\gamma)E^b_\beta E^c_\gamma e^{-i\omega_\Sigma t}. \end{aligned} \tag{87}$$

For a monochromatic field with $\omega_\beta = -\omega_\gamma = \omega$ and $\omega_\Sigma = 0$, we have

$$\begin{aligned} \eta_{abc}(0;\omega,-\omega) &= \frac{\pi e^3}{2\hbar^2}\sum_{nm}\int_k \Delta^a_{nm}f_{nm}(\mathcal{A}^b_{mn}\mathcal{A}^c_{nm} - \mathcal{A}^c_{mn}\mathcal{A}^b_{nm})\delta(\omega_{mn}-\omega) \\ &= -\frac{i\pi e^3}{2\hbar^2}\sum_{nm}\int_k \Delta^a_{nm}f_{nm}\Omega^{bc}_{mn}\delta(\omega_{mn}-\omega), \end{aligned} \tag{88}$$

which recovers Eq. (64), which is the result in the length gauge.

Appendix 3: Derivation of MR-induced nonlinear current for the four-band model

Here we drive the MR-induced nonlinear current for the four-band model Eq. (1). Following the same procedure in Appendix 2, we find the second-quantized Hamiltonian as follows

$$\hat{H} = \sum_n \int d\boldsymbol{k}\varepsilon_{n\boldsymbol{k}}\hat{a}^\dagger_{n\boldsymbol{k}}\hat{a}_{n\boldsymbol{k}} + \sum_{nn'}\int d\boldsymbol{k}\hat{a}^\dagger_{n\boldsymbol{k}}\hat{a}_{n'\boldsymbol{k}}[\boldsymbol{A}(t)\cdot\boldsymbol{J}_{nn'\boldsymbol{k}} + \boldsymbol{v}(t)\cdot\boldsymbol{\Gamma}_{nn'\boldsymbol{k}}], \tag{89}$$

where $\varepsilon_{n\boldsymbol{k}}$ is the eigenvalue of H_0, $\boldsymbol{J}$ is the current operator, and $\boldsymbol{\Gamma} = \boldsymbol{\sigma}\tau_z$. We then obtain the first-order and second-order intraband density operator

$$\rho^{(1)}_{nm}(\omega) = f_{nm}\frac{A^b(\omega)J^b_{mn} + v^b(\omega)\Gamma^b_{mn}}{\hbar(\tilde{\omega}_{1,nm}-\omega)}, \tag{90}$$

$$\begin{aligned} \rho^{(2)}_{nn}(\omega_\Sigma) = \frac{1}{\hbar\omega_\Sigma}\sum_m A^b_\beta v^c_\gamma\left[\frac{f_{mn}J^b_{mn}\Gamma^c_{nm}}{\hbar(\tilde{\omega}_{1,mn}-\omega_\beta)} - \frac{f_{nm}J^b_{nm}\Gamma^c_{mn}}{\hbar(\tilde{\omega}_{1,nm}-\omega_\beta)}\right] \\ + v^b_\beta A^c_\gamma\left[\frac{f_{mn}\Gamma^b_{mn}J^c_{nm}}{\hbar(\tilde{\omega}_{1,mn}-\omega_\beta)} - \frac{f_{nm}\Gamma^b_{nm}J^c_{mn}}{\hbar(\tilde{\omega}_{1,nm}-\omega_\beta)}\right]. \end{aligned} \tag{91}$$

The current reads

$$\begin{aligned} \tilde{j}^a(t) &= \frac{e}{\hbar^2\omega_\Sigma}\sum_{nm}\int_k \frac{\Delta^a_{nm}f_{mn}}{\tilde{\omega}_{1,mn}-\omega_\beta}\left[J^b_{mn}\Gamma^c_{nm}A^b_\beta v^c_\gamma + \Gamma^b_{mn}J^c_{nm}v^b_\beta A^c_\gamma\right]e^{-i\omega_\Sigma t} \\ &= \frac{e^2}{\hbar^3\omega_\Sigma}\sum_{nm}\int_k \frac{\Delta^a_{nm}f_{mn}}{\tilde{\omega}_{1,mn}-\omega_\beta}\left[\frac{J^b_{mn}\Gamma^c_{nm}}{\omega_\beta\omega_\gamma}E^b_\beta\tilde{E}^c_\gamma + \frac{\Gamma^b_{mn}J^c_{nm}}{\omega_\beta\omega_\gamma}\tilde{E}^b_\beta E^c_\gamma\right]e^{-i\omega_\Sigma t}, \end{aligned} \tag{92}$$

where $\tilde{E}^b_\beta = i\hbar\omega_\beta v^b_\beta/e$ is the pseudo-electric field. Next we take the imaginary part and the time derivative of the current, and for $\omega_\beta = -\omega_\gamma = \omega$, we have

$$\frac{d\tilde{j}^a(t)}{dt} = \tilde{\eta}_{abc}(0;\omega,-\omega)E_b(\omega)\tilde{E}_c(-\omega) + \tilde{\eta}_{acb}(0;-\omega,\omega)\tilde{E}_b(\omega)E_c(-\omega), \tag{93}$$

with

$$\begin{aligned} \tilde{\eta}_{abc}(0;\omega,-\omega) &= \frac{\pi e^2}{\hbar^3}\sum_{nm}\int_k \Delta^a_{nm}f_{nm}\frac{J^b_{mn}\Gamma^c_{nm}}{\omega^2}\delta(\omega_{mn}-\omega) \\ &= \frac{i\pi e^3}{\hbar^2}\sum_{nm}\int\frac{d^3k}{(2\pi)^3}(\partial_a\varepsilon_{nm})f_{nm}\frac{\mathcal{A}^b_{nm}\Gamma^c_{mn}}{\varepsilon_{nm}}\delta(\varepsilon_{mn}-\hbar\omega), \end{aligned} \tag{94}$$

where $\tilde{\boldsymbol{E}}(\omega)$ is defined as $i\hbar\omega\boldsymbol{v}/e$.

Appendix 4: Derivation of the Landau-Lifshitz-Gilbert Equation for ferromagnetic resonance

Following Eq. (26) in Section 4, we perform the Laplace transformation as

$$\begin{aligned}\tilde{n}_i(s) &= \int_0^\infty dt e^{-st} n_i(t),\\ \tilde{B}_i(s) &= \int_0^\infty dt e^{-st} B_i(t).\end{aligned} \tag{95}$$

Equation (26) then becomes

$$G_0(s)\begin{pmatrix}\tilde{n}_x(s)\\ t n_y(s)\end{pmatrix} - \begin{pmatrix}n_x(0)\\ n_y(0)\end{pmatrix} = G_1\begin{pmatrix}\tilde{B}_x(s)\\ \tilde{B}_y(s)\end{pmatrix}, \tag{96}$$

where

$$G_0(s) = \begin{pmatrix}s+\alpha\tilde{\omega} & \tilde{\omega}n_z\\ -\tilde{\omega}n_z & s+\alpha\tilde{\omega}\end{pmatrix},\ G_1 = \begin{pmatrix}\gamma\alpha & \gamma n_z\\ -\gamma n_z & \gamma\alpha\end{pmatrix}. \tag{97}$$

We consider a general in-plane magnetic field $\boldsymbol{B}(t) = B_0 e^{i\omega t}(a, b, 0)$ where a, b are two complex numbers and describe the polarization of magnetic field components of a microwave. The transformed field reads

$$\begin{aligned}\tilde{B}_x(s) &= \frac{B_0}{2}\left(\frac{a}{s-i\omega} + \frac{a^*}{s+i\omega}\right),\\ \tilde{B}_y(s) &= \frac{B_0}{2}\left(\frac{b}{s-i\omega} + \frac{b^*}{s+i\omega}\right).\end{aligned} \tag{98}$$

We then perform the inverse Laplace transformation on Eq. (96) and obtain

$$\begin{aligned}\begin{pmatrix}n_x\\ n_y\end{pmatrix} &= \frac{B_0}{2}\left[a e^{i\omega t} G_0^{-1}(i\omega) + a^* e^{-i\omega t} G_0^{-1}(-i\omega)\right] G_1\begin{pmatrix}1\\ 0\end{pmatrix}\\ &+ \frac{B_0}{2}\left[b e^{i\omega t} G_0^{-1}(i\omega) + b^* e^{-i\omega t} G_0^{-1}(-i\omega)\right] G_1\begin{pmatrix}0\\ 1\end{pmatrix},\end{aligned} \tag{99}$$

where

$$G_0^{-1}(s) = \frac{1}{(s+\alpha\tilde{\omega})^2 + \tilde{\omega}^2}\begin{pmatrix}s+\alpha\tilde{\omega} & -\tilde{\omega}n_z\\ \tilde{\omega}n_z & s+\alpha\tilde{\omega}\end{pmatrix}. \tag{100}$$

The solutions to the above equation are

$$\begin{aligned}n_x(t) &= \frac{B_0\gamma}{2D(\omega)}[A_1(\omega)\cos(\omega t) + A_2(\omega)\sin(\omega t)]\\ A_1(\omega) &= ((\alpha^2+1)\tilde{\omega}^2 - \omega^2)\left[(a+a^*)(\alpha^2+1)\tilde{\omega} + i\omega((a-a^*)\alpha + (b-b^*)n_z)\right]\\ &- 2i\alpha\omega\tilde{\omega}\left[(a-a^*)(\alpha^2+1)\tilde{\omega} + i\omega((a+a^*)\alpha + (b+b^*)n_z)\right]\\ A_2(\omega) &= ((\alpha^2+1)\tilde{\omega}^2 - \omega^2)\left[i(a-a^*)(\alpha^2+1)\tilde{\omega} - \omega((a+a^*)\alpha + (b+b^*)n_z)\right]\\ &- 2i\alpha\omega\tilde{\omega}\left[i(a+a^*)(\alpha^2+1)\tilde{\omega} + \omega((a^*-a)\alpha + (b^*-b)n_z)\right],\end{aligned} \tag{101}$$

and

$$\begin{aligned}n_y(t) &= \frac{B_0\gamma}{2D(\omega)}[A_3(\omega)\cos(\omega t) + A_4(\omega)\sin(\omega t)]\\ A_3(\omega) &= ((\alpha^2+1)\tilde{\omega}^2 - \omega^2)\left[(b+b^*)(\alpha^2+1)\tilde{\omega} + i\omega((b-b^*)\alpha + (a^*-a)n_z)\right]\\ &- 2i\alpha\omega\tilde{\omega}\left[(b-b^*)(\alpha^2+1)\tilde{\omega} + i\omega((b+b^*)\alpha - (a+a^*)n_z)\right]\\ A_4(\omega) &= ((\alpha^2+1)\tilde{\omega}^2 - \omega^2)\left[i(b-b^*)(\alpha^2+1)\tilde{\omega} - \omega((b+b^*)\alpha - (a+a^*)n_z)\right]\\ &- 2i\alpha\omega\tilde{\omega}\left[i(b+b^*)(\alpha^2+1)\tilde{\omega} + \omega((b^*-b)\alpha + (a-a^*)n_z)\right],\end{aligned} \tag{102}$$

where

$$D(\omega) = (\alpha^2+1)^2\tilde{\omega}^4 + \omega^4 + 2(\alpha^2-1)\tilde{\omega}^2\omega^2. \tag{103}$$

We find the resonance frequency satisfying $D(\omega_r) = 0$ to be

$$\omega_r = \sqrt{\frac{\sqrt{(\alpha^2+1)^2(4\alpha^2+1)} - (\alpha^2+1)^2}{\alpha^2}}|\tilde{\omega}|. \tag{104}$$

Acknowledgements
We thank Binghai Yan and Jiabin Yu for helpful discussion.

Author contributions
C.X.L conceived the original idea and supervised the whole project. R. M performed the theoretical analysis and the numerical simulations. Both authors contributed essentially to the manuscript preparation.

Funding
R. M and C.X.L acknowledge the support from the NSF through The Pennsylvania State University Materials Research Science and Engineering Center [DMR-2011839]. C.X.L also acknowledge the support from NSF Grant No. DMR-2241327.

Data availability
Data and codes generated during this study are available upon request to the corresponding author.

Declarations

Competing interests
The authors declare that they have no competing interests.

Received: 14 November 2024 Accepted: 11 February 2025
Published online: 25 February 2025

References

1. M.V. Berry, Quantal phase factors accompanying adiabatic changes. Proc. R. Soc. Lond. A. Math. Phys. Sci. **392**, 45 (1984)
2. D. Xiao, M.-C. Chang, Q. Niu, Berry phase effects on electronic properties. Rev. Mod. Phys. **82**, 1959 (2010)
3. T. Liu, X.-B. Qiang, H.-Z. Lu, X. Xie, Quantum geometry in condensed matter. Natl. Sci. Rev. **12**, nwae334 (2024)
4. R. Resta, The insulating state of matter: a geometrical theory. Eur. Phys. J. B **79**, 121 (2011)
5. P. Törmä, Essay: Where can quantum geometry lead us? Phys. Rev. Lett. **131**, 240001 (2023)
6. J. Provost, G. Vallee, Riemannian structure on manifolds of quantum states. Commun. Math. Phys. **76**, 289 (1980)
7. D.J. Thouless, M. Kohmoto, M.P. Nightingale, M. den Nijs, Quantized Hall conductance in a two-dimensional periodic potential. Phys. Rev. Lett. **49**, 405 (1982)

8. I. Sodemann, L. Fu, Quantum nonlinear Hall effect induced by Berry curvature dipole in time-reversal invariant materials. Phys. Rev. Lett. **115**, 216806 (2015)
9. Z. Du, H.-Z. Lu, X. Xie, Nonlinear Hall effects. Nat. Rev. Phys. **3**, 744 (2021)
10. Y. Zhang, Y. Sun, B. Yan, Berry curvature dipole in Weyl semimetal materials: an ab initio study. Phys. Rev. B **97**, 041101 (2018)
11. C. Wang, Y. Gao, D. Xiao, Intrinsic nonlinear hall effect in antiferromagnetic tetragonal cumnas. Phys. Rev. Lett. **127**, 277201 (2021)
12. K. Das, S. Lahiri, R.B. Atencia, D. Culcer, A. Agarwal, Intrinsic nonlinear conductivities induced by the quantum metric. Phys. Rev. B **108**, L201405 (2023)
13. D. Kaplan, T. Holder, B. Yan, Unification of nonlinear anomalous Hall effect and nonreciprocal magnetoresistance in metals by the quantum geometry. Phys. Rev. Lett. **132**, 026301 (2024)
14. Q. Ma, S.-Y. Xu, H. Shen, D. MacNeill, V. Fatemi, T.-R. Chang, A.M. Mier Valdivia, S. Wu, Z. Du, C.-H. Hsu et al., Observation of the nonlinear Hall effect under time-reversal-symmetric conditions. Nature **565**, 337 (2019)
15. K. Kang, T. Li, E. Sohn, J. Shan, K.F. Mak, Nonlinear anomalous Hall effect in few-layer WTe_2. Nat. Mater. **18**, 324 (2019)
16. O.O. Shvetsov, V.D. Esin, A.V. Timonina, N.N. Kolesnikov, E. Deviatov, Nonlinear Hall effect in three-dimensional Weyl and Dirac semimetals. JETP Lett. **109**, 715 (2019)
17. S. Dzsaber, X. Yan, M. Taupin, G. Eguchi, A. Prokofiev, T. Shiroka, P. Blaha, O. Rubel, S.E. Grefe, H.-H. Lai et al., Giant spontaneous Hall effect in a nonmagnetic Weyl-Kondo semimetal. Proc. Natl. Acad. Sci. **118**, e2013386118 (2021)
18. M.-S. Qin, P.-F. Zhu, X.-G. Ye, W.-Z. Xu, Z.-H. Song, J. Liang, K. Liu, Z.-M. Liao, Strain tunable Berry curvature dipole, orbital magnetization and nonlinear Hall effect in WSe_2 monolayer. Chin. Phys. Lett. **38**, 017301 (2021)
19. A. Tiwari, F. Chen, S. Zhong, E. Drueke, J. Koo, A. Kaczmarek, C. Xiao, J. Gao, X. Luo, Q. Niu et al., Giant c-axis nonlinear anomalous hall effect in Td-$MoTe_2$ and WTe_2. Nat. Commun. **12**, 2049 (2021)
20. T. Ma, H. Chen, K. Yananose, X. Zhou, L. Wang, R. Li, Z. Zhu, Z. Wu, Q.-H. Xu, J. Yu et al., Growth of bilayer $MoTe_2$ single crystals with strong non-linear Hall effect. Nat. Commun. **13**, 5465 (2022)
21. M. Huang, Z. Wu, X. Zhang, X. Feng, Z. Zhou, S. Wang, Y. Chen, C. Cheng, K. Sun, Z.Y. Meng et al., Intrinsic nonlinear Hall effect and gate-switchable Berry curvature sliding in twisted bilayer graphene. Phys. Rev. Lett. **131**, 066301 (2023)
22. M. Huang, Z. Wu, J. Hu, X. Cai, E. Li, L. An, X. Feng, Z. Ye, N. Lin, K. T. Law et al., Giant nonlinear Hall effect in twisted bilayer WSe_2. Natl. Sci. Rev. **10**, nwac232 (2023)
23. Y. Zhao, J. Cao, Z. Zhang, S. Li, Y. Li, F. Ma, S.A. Yang, Berry curvature dipole and nonlinear Hall effect in two-dimensional $Nb_{2n+1}Si_nTe_{4n+2}$. Phys. Rev. B **107**, 205124 (2023)
24. A. Gao, Y.-F. Liu, J.-X. Qiu, B. Ghosh, T.V. Trevisan, Y. Onishi, C. Hu, T. Qian, H.-J. Tien, S.-W. Chen et al., Quantum metric nonlinear Hall effect in a topological antiferromagnetic heterostructure. Science **381**, 181 (2023)
25. N. Wang, D. Kaplan, Z. Zhang, T. Holder, N. Cao, A. Wang, X. Zhou, F. Zhou, Z. Jiang, C. Zhang et al., Quantum-metric-induced nonlinear transport in a topological antiferromagnet. Nature **621**, 487 (2023)
26. C. Le, Y. Zhang, C. Felser, Y. Sun, Ab initio study of quantized circular photogalvanic effect in chiral multifold semimetals. Phys. Rev. B **102**, 121111 (2020)
27. F. de Juan, A.G. Grushin, T. Morimoto, J.E. Moore, Quantized circular photogalvanic effect in Weyl semimetals. Nat. Commun. **8**, 15995 (2017)
28. C. Le, Y. Sun, Topology and symmetry of circular photogalvanic effect in the chiral multifold semimetals: a review. J. Phys. Condens. Matter **33**, 503003 (2021)
29. D. Rees, K. Manna, B. Lu, T. Morimoto, H. Borrmann, C. Felser, J. Moore, D.H. Torchinsky, J. Orenstein, Helicity-dependent photocurrents in the chiral weyl semimetal RhSi. Sci. Adv. **6**, eaba0509 (2020)
30. Z. Ni, K. Wang, Y. Zhang, O. Pozo, B. Xu, X. Han, K. Manna, J. Paglione, C. Felser, A.G. Grushin et al., Giant topological longitudinal circular photogalvanic effect in the chiral multifold semimetal CoSi. Nat. Commun. **12**, 154 (2021)
31. Z. Ni, B. Xu, M.-Á. Sánchez-Martínez, Y. Zhang, K. Manna, C. Bernhard, J. Venderbos, F. De Juan, C. Felser, A. G. Grushin et al., Linear and nonlinear optical responses in the chiral multifold semimetal RhSi. npj Quantum Mater. **5**, 96 (2020)
32. Z. Ji, G. Liu, Z. Addison, W. Liu, P. Yu, H. Gao, Z. Liu, A.M. Rappe, C.L. Kane, E.J. Mele et al., Spatially dispersive circular photogalvanic effect in a Weyl semimetal. Nat. Mater. **18**, 955 (2019)
33. Q. Ma, A.G. Grushin, K.S. Burch, Topology and geometry under the nonlinear electromagnetic spotlight. Nat. Mater. **20**, 1601 (2021)
34. F. Flicker, F. De Juan, B. Bradlyn, T. Morimoto, M.G. Vergniory, A.G. Grushin, Chiral optical response of multifold fermions. Phys. Rev. B **98**, 155145 (2018)
35. Y. Zhang, H. Ishizuka, J. van den Brink, C. Felser, B. Yan, N. Nagaosa, Photogalvanic effect in Weyl semimetals from first principles. Phys. Rev. B **97**, 241118 (2018)
36. A. Avdoshkin, V. Kozii, J.E. Moore, Interactions remove the quantization of the chiral photocurrent at Weyl points. Phys. Rev. Lett. **124**, 196603 (2020)
37. A.-K. Wu, D. Guerci, Y. Fu, J.H. Wilson, J. Pixley, Absence of quantization in the circular photogalvanic effect in disordered chiral Weyl semimetals. Phys. Rev. B **110**, 014201 (2024)
38. J. Yu, J. Zang, C.-X. Liu, Magnetic resonance induced pseudoelectric field and giant current response in axion insulators. Phys. Rev. B **100**, 075303 (2019)
39. J. Yu, C.-X. Liu, in *Semiconductors and Semimetals*. Pseudo-gauge fields in Dirac and Weyl materials, vol. 108 (Elsevier, Cambridge, 2021) pp. 195–224
40. R. Ilan, A.G. Grushin, D.I. Pikulin, Pseudo-electromagnetic fields in 3d topological semimetals. Nat. Rev. Phys. **2**, 29 (2020)
41. C.-X. Liu, P. Ye, X.-L. Qi, Chiral gauge field and axial anomaly in a Weyl semimetal. Phys. Rev. B **87**, 235306 (2013)
42. N. Armitage, E. Mele, A. Vishwanath, Weyl and dirac semimetals in three-dimensional solids. Rev. Mod. Phys. **90**, 015001 (2018)
43. C. Kittel, P. McEuen, *Introduction to solid state physics*, vol. 8 (Wiley, New York, 1976)
44. A. Aharoni, *Introduction to the Theory of Ferromagnetism*, vol. 109 (Clarendon Press, Oxford, 2000)
45. C. Aversa, J.E. Sipe, Nonlinear optical susceptibilities of semiconductors: Results with a length-gauge analysis. Phys. Rev. B **52**, 14636 (1995)
46. G. Ventura, D. Passos, J.L. Dos Santos, J.V.P. Lopes, N.M. Peres, Gauge covariances and nonlinear optical responses. Phys. Rev. B **96**, 035431 (2017)
47. J. Sipe, A. Shkrebtii, Second-order optical response in semiconductors. Phys. Rev. B **61**, 5337 (2000)
48. H. Chen, M. Ye, N. Zou, B.-L. Gu, Y. Xu, W. Duan, Basic formulation and first-principles implementation of nonlinear magneto-optical effects. Phys. Rev. B **105**, 075123 (2022)
49. D.E. Parker, T. Morimoto, J. Orenstein, J.E. Moore, Diagrammatic approach to nonlinear optical response with application to Weyl semimetals. Phys. Rev. B **99**, 045121 (2019)
50. D. Passos, G. Ventura, J.V.P. Lopes, J.L. Dos Santos, N. Peres, Nonlinear optical responses of crystalline systems: Results from a velocity gauge analysis. Phys. Rev. B **97**, 235446 (2018)

Publisher's Note